

Measuring Distances and Probing the Unresolved Stellar Populations of Galaxies Using Infrared Surface Brightness Fluctuations¹

Joseph B. Jensen

Gemini Observatory, 670 N. A'ohoku Pl., Hilo, HI 96720
jjensen@gemini.edu

John L. Tonry and Brian J. Barris

Institute for Astronomy, University of Hawaii
2680 Woodlawn Drive, Honolulu, HI 96822
jt@avidya.ifa.hawaii.edu, barris@ifa.hawaii.edu

Rodger I. Thompson

Steward Observatory, University of Arizona, Tucson, AZ 85721
rthompson@as.arizona.edu

Michael C. Liu²

Institute for Astronomy, University of Hawaii
2680 Woodlawn Drive, Honolulu, HI 96822
mliu@ifa.hawaii.edu

Marcia J. Rieke

Steward Observatory, University of Arizona, Tucson, AZ 85721
mrieke@as.arizona.edu

Edward A. Ajhar

University of Miami, Department of Physics
1320 Campo Sano Drive, Coral Gables, FL 33146
ajhar@physics.miami.edu

and

John P. Blakeslee

Johns Hopkins University, Department of Physics and Astronomy
3400 North Charles Street, Baltimore, MD 21218-2686
jpb@pha.jhu.edu

ABSTRACT

To empirically calibrate the IR surface brightness fluctuation (SBF) distance scale and probe the properties of unresolved stellar populations, we measured fluctuations in 65 galaxies using NICMOS on the *Hubble Space Telescope*. The early-type galaxies in this sample include elliptical and S0 galaxies and spiral bulges in a variety of environments. Absolute fluctuation magnitudes in the F160W (1.6 μm) filter ($\overline{M}_{\text{F160W}}$) were derived for each galaxy using previously-measured *I*-band SBF and Cepheid variable star distances. F160W SBFs can be used to measure distances to early-type galaxies with a relative accuracy of $\sim 10\%$ provided that the galaxy color is known to ~ 0.035 mag or better. Near-IR fluctuations can also reveal the properties of the most luminous stellar populations in galaxies. Comparison of F160W fluctuation magnitudes and optical colors to stellar population model predictions suggests that bluer elliptical and S0 galaxies have significantly younger populations than redder ones, and may also be more metal-rich. There are no galaxies in this sample with fluctuation magnitudes consistent with old, metal-poor ($t > 5$ Gyr, $[\text{Fe}/\text{H}] < -0.7$) stellar population models. Composite stellar population models imply that bright fluctuations in the bluer galaxies may be the result of an episode of recent star formation in a fraction of the total mass of a galaxy. Age estimates from the F160W fluctuation magnitudes are consistent with those measured using the $\text{H}\beta$ Balmer line index. The two types of measurements make use of completely different techniques and are sensitive to stars in different evolutionary phases. Both techniques reveal the presence of intermediate-age stars in the early-type galaxies of this sample.

Subject headings: galaxies: evolution — galaxies: stellar content — galaxies: distances and redshifts

1. Introduction

The techniques for measuring surface brightness fluctuations (SBFs) were developed primarily with the goal of determining extragalactic distances. The optical SBF method

¹Based on observations with the NASA/ESA Hubble Space Telescope, obtained at the Space Telescope Science Institute, which is operated by AURA, Inc., under NASA contract NAS 5-26555.

²Beatrice Watson Parrent Fellow

has proven to be remarkably useful for estimating distances (see Blakeslee et al. 1999 for a review). The initial motivation for extending ground-based SBF measurements to near-IR wavelengths was to take advantage of intrinsically brighter fluctuations and better atmospheric seeing to reach much greater distances (Jensen et al. 2001, hereafter J2001; Jensen, Tonry, & Luppino 1999; Liu & Graham 2001). With *Hubble Space Telescope's* (HST) Near Infrared Camera and Multi-Object Spectrometer (NICMOS), the low background and lack of atmospheric seeing offer significant advantages over ground-based IR SBF measurements.

Accurate SBF distance measurements rely on the empirical calibration of absolute fluctuation amplitudes. Several studies have used observations of galaxies with previously-measured distances to determine absolute fluctuation magnitudes, which were found to agree with the predictions of stellar population models. The first IR SBF measurements were made by Luppino & Tonry (1993), who found that M32 has a somewhat brighter (~ 0.25 mag) K -band SBF magnitude than the bulge of M31. Pahre & Mould (1994) measured K -band SBF magnitudes for a sample of Virgo galaxies, and found that two of eight had significantly brighter ($\gtrsim 1$ mag) fluctuations than the others. Pahre & Mould's results were confirmed by Jensen, Luppino, & Tonry (1996) in their sample of seven Virgo cluster elliptical galaxies. The IR SBF signal for one of the two anomalous galaxies (NGC 4365) was later found to have been over-estimated due to the contribution of undetected globular clusters (Jensen, Tonry, & Luppino 1998); the other (NGC 4489) still appeared to have brighter fluctuations than the others.

To the 1996 Virgo sample, Jensen et al. (1998) added galaxies in the Fornax and Eridanus clusters. Three of the bluest galaxies in their sample showed K -band fluctuation magnitudes that were ~ 0.25 mag brighter than the others. Jensen et al. noted that the models implied younger stellar populations in these bluer ellipticals. However, the sample size was small and the range in $(V-I)$ color was limited; hence, the slope they measured was not statistically significant and they adopted a constant K -band SBF calibration. The K -band fluctuations for the bluest galaxy in their sample (NGC 4489) were significantly brighter than the others in the Virgo cluster, but the measurement was not trusted due to its low signal-to-noise (S/N) ratio. Mei, Silva, & Quinn (2001c) subsequently re-observed this galaxy and found comparably bright K -band fluctuations.

Recently, a larger sample of K -band SBF magnitudes for Fornax cluster galaxies has been measured by Liu, Graham, & Charlot (2002). Combined with the previously published data, the resulting sample covered a much larger range of galaxy properties (e.g., color and luminosity). Liu et al. (2002) discovered that the brighter K -band fluctuations seen in bluer galaxies in their sample and in earlier data sets (Luppino & Tonry 1993; Pahre & Mould 1994; Jensen et al. 1998) were correlated with $(V-I)$. Liu et al. found the K -band slope

with color to be comparable to that for I -band SBFs. This relation naturally explained the bright IR SBFs previously measured in M32 (Luppino & Tonry 1993) and NGC 4489 (Mei et al. 2001c). Moreover, a generic prediction of IR SBF models is that IR fluctuations are sensitive to variations in the ages and metallicities of stellar populations. Hence, the discovery of a *systematic* relation between IR SBFs and galaxy color means that age and metallicity are related in a way that reflects the star formation history of a galaxy. Liu et al. (2002) concluded that early-type galaxies in clusters have a significant spread in age and approximately solar metallicities.

Liu et al. (2002) also reported finding three Fornax cluster galaxies with K -band fluctuation magnitudes brighter than the other galaxies with similar $(V-I)$ colors. These galaxies were not included in their calibration fit. They are primarily lower luminosity galaxies, and models suggest the presence of a high-metallicity burst of star formation in the last few Gyr. Mei et al. (2001a) have confirmed that one of the three Fornax galaxies (NGC 1427) has unusually bright K -band fluctuations.

To calibrate the F160W ($1.6 \mu\text{m}$) SBF distance scale and better understand the nature of the bluer, low-luminosity elliptical galaxies, we measured F160W SBF magnitudes in a large sample of 65 galaxies spanning a wide range in color ($(V-I)_0 = 1.05$ to 1.28). All the data presented here were obtained using the NIC2 camera of NICMOS. The data are of uniform image quality, and the S/N ratios are large. Many of the galaxy images were collected for other programs and retrieved from the public archive.

Distances to the galaxies in this sample were taken from the growing collection of Cepheid variable star distances measured with the *HST* (Freedman et al. 2001, Ferrarese et al. 2000b; Gibson & Stetson 2001; Saha et al. 2001), and from the extensive I -band SBF survey (Tonry et al. 2001; Ajhar et al. 1997; Lauer et al. 1998; Tonry et al. 1997). The I -band SBF distances used here were calibrated using Cepheid distances to the same galaxies; no assumptions about group or cluster membership were made (Tonry et al. 2001). For the current study we shifted the I -SBF distances published by Tonry et al. by -0.16 mag to the new Cepheid zero point of Freedman et al. (2001), which makes use of the improved Cepheid period-luminosity relations published by Udalski et al. (1999). The distances presented in this paper, whether from Cepheids directly or from I -band SBFs, are subject to the systematic uncertainties in the Cepheid distance scale (Ferrarese et al. 2000a). We adopted a distance modulus to the Large Magellanic Cloud (LMC) of 18.50 mag (Freedman et al. 2001; Carretta et al. 2000), and acknowledge that the continuing debate over the LMC distance remains one of the largest sources of systematic uncertainty.

In this paper we present a new calibration of the F160W distance scale and explore its sensitivity to galaxy color. We also compare the absolute fluctuation magnitudes to those

predicted by three sets of stellar population models: the widely-used models of Worthey (1994), the Bruzual & Charlot (1993, 2002) models (as published by Liu, Charlot, & Graham 2000 and Liu et al. 2002), and the Vazdekis (1999, 2001) models (as published by Blakeslee, Vazdekis, & Ajhar 2001). SBF ages determined using stellar population models are compared with those measured using the age-sensitive $H\beta$ Balmer line strength.

2. Observations

2.1. F160W SBF Measurements

The observations of galaxies used in this study come from two basic types of NICMOS program, each of which accounts for roughly half the data. The first set of observations came from two programs explicitly designed for SBF measurements. The first of these (NICMOS program ID 7453) targeted galaxies in Virgo, Leo, and Fornax to empirically calibrate the F160W SBF distance scale for more distant measurements. The second (program ID 7458) measured fluctuations in a large sample of Fornax galaxies at multiple wavelengths to better understand stellar populations. A subset of the measurements presented in this paper was published by J2001. The second category of observations is comprised of data taken from the public archive from a variety of programs. Most of these are short, “snapshot” survey images of the centers of galaxies, and have only a minimal number of individual exposures. Observational data are listed in Table 1.

The observations presented in this study were taken with the NIC2 camera (19.2 arcsec field of view) through the F160W filter. F160W NIC2 observations of approximately 300 galaxies with heliocentric redshifts less than $10,000 \text{ km s}^{-1}$ were retrieved from the public archive and examined. A smooth fit to each galaxy was subtracted from the pipeline-reduced image and the residual frame examined. All the galaxies that were judged to be hopelessly dusty were rejected from further consideration. Data for the remaining ~ 200 galaxies were reduced again from the raw data and the SBF analysis completed following the same procedures as described by J2001. The subset of 65 galaxies presented here are those for which reliable distances are known from either Cepheid variable stars or I -band SBFs.

The methodology for determining F160W fluctuation magnitudes was very similar to that described by J2001, with some simplifications. We used the software developed by the NICMOS GTO team to prepare the images for analysis (Thompson et al. 1999). Dark current was first subtracted from the raw NIC2 F160W images. The multiple reads of each MULTIACCUM sequence were combined and cosmic rays identified and removed. Adjustment of the bias pedestal for each quadrant was performed as described by J2001, although

it was unnecessary in most cases. Exposures from individual telescope pointings were flat field corrected and combined. Residual images from cosmic rays were not a significant source of contamination in these high- S/N ratio data.

The photometric zero point used by J2001 was determined by M. Rieke and the NICMOS team. Additional standard star measurements combined with a better tie to ground-based photometry has yielded a better zero point for the NIC2 F160W filter. The new photometric zero point that we adopted for this study is 0.033 mag fainter than that used by J2001. The new calibration for NIC2 is 2.126×10^{-6} Jy ADU $^{-1}$ s $^{-1}$. The magnitude zero point on the Vega system is 1083 Jy. This new calibration is within the uncertainty in zero point published by J2001. If the current zero point were applied to the J2001 data without any other changes to the calibration, the resulting fluctuation magnitudes would be 0.03 mag fainter, and the Hubble constant would be larger by 1.6%. SBF magnitudes were corrected for Galactic extinction using the measurements of Schlegel, Finkbeiner, & Davis (1998). We adopted $A_B = 4.315 E(B-V)$ and $A_H = 0.132 A_B$ (Schlegel et al 1998).

The galaxies in this sample are much closer than the distant galaxies used by J2001 to determine the Hubble constant (5 included here were taken from the intermediate-distance sample of J2001). The median S/N ratio was 16 per pixel for this data set, which, given the large number of pixels sampled, is more than sufficient to achieve a highly-reliable measurement. Most of the data had S/N ratios between 10 and 20; the full range includes measurements with S/N ratios as low as 5 and as high as 4000. The fluctuation power was determined by fitting the scaled power spectrum of the reference point-spread function (PSF) to the spatial power spectrum of the cleaned and galaxy-subtracted data. The library of empirical PSF stars collected as part of the IR SBF Hubble constant project (J2001) was used to perform the SBF analysis. A full discussion of the techniques for calculating fluctuation magnitudes \overline{m}_{F160W} from NICMOS data is presented by J2001.

We found that correcting the F160W SBF magnitudes for undetected globular clusters or background galaxies was unnecessary for the relatively-nearby galaxies of this study because the stellar SBF signal always dominated over other sources of variance. The final galaxy-subtracted images were masked of visible point sources and dusty regions before proceeding with the SBF analysis. Only the five intermediate-distance galaxies from J2001 required corrections for undetected globular clusters, background galaxies, and residual background patterns (as described by J2001).

The uncertainties in apparent fluctuation magnitudes \overline{m}_{F160W} were typically 0.1 mag or less. The primary components of the uncertainty were the fit to fluctuation power and the PSF normalization (usually 0.05 mag each). The contribution from sky subtraction was much smaller (typically 0.01 mag). Contributions to the uncertainty from undetected

globular clusters or background galaxies were negligible (<0.01 mag), and contaminating power from residual cosmic rays or incomplete bias subtraction were unmeasurable in these high- S/N ratio measurements.

2.2. Distances and Absolute Fluctuation Magnitudes

Computing the absolute fluctuation magnitudes \overline{M}_{F160W} for the galaxies in our sample required independent distance measurements. All the distance moduli used in this study (Table 2) were based, either directly or indirectly, on Cepheid variable star distances. Two classes of distance measurements are presented here: first, a large set of 61 I -band SBF distances (calibrated using Cepheid distances as described by Tonry et al. 1997), and second, a smaller set of nine Cepheid distances measured using WFPC2 on the *HST*.

Because only a few of the spiral galaxies with measured Cepheid distances have smooth, dust-free regions appropriate for SBF analysis, the majority of the absolute fluctuation magnitudes presented in this paper were computed using I -band SBF distances (Tonry et al. 2001). Most of the I -band SBF distance measurements were made using ground-based telescopes, but five galaxies were observed using WFPC2 (J2001; Lauer et al. 1998; Ajhar et al. 1997). The empirical I -band SBF calibration (Tonry et al. 1997) adopted for this study used Cepheid and I -SBF distance measurements to seven galaxies for which both types of measurement are possible. No assumptions about group or cluster membership were made to connect the Cepheid and I -band SBF distance scales. The original Key Project calibration of the Cepheid distance scale (Ferrarese et al. 2000b, Freedman & Madore 1990) was used for the empirical I -band SBF calibration presented by Tonry et al. (1997, 2001). For the I -band SBF distances presented here we have updated the zero point using the greatly-improved period-luminosity relations determined by Udalski et al. (1999) using 650 LMC Cepheids. The new period-luminosity relation results in a shift of -0.16 mag in the distance moduli of all the I -band SBF galaxies. No metallicity correction to the Cepheid distances is adopted for this study.

The modifications to the period–luminosity relation adopted by Freedman et al. (2001) are distance dependent. The new period–luminosity relation is different for the I -band, while at V it is unchanged (Udalski et al. 1999). The effect is that the new period–luminosity relation predicts higher reddening corrections for redder Cepheids, and therefore smaller distances. The effect is largest in Cepheids with longer periods. Because only the brightest (longest-period) Cepheids are detected in the most distant galaxies, the offset between the previously-published distances and those derived using the new calibration are largest in the most distant galaxies (~ 0.2 mag, or 10% in distance). The offset to the I -band SBF

calibration due to the new period-luminosity relation is 0.16 mag, or 8% in distance.

Nine galaxies in the F160W NICMOS sample have Cepheid distances measured using HST (Ferrarese et al. 2000b; Freedman et al. 1994, 2001; Gibson & Stetson 2001; Gibson et al. 1999, 2000; Graham et al. 1997; Saha et al. 1996, 2001). A distance modulus to the LMC of 18.50 mag was adopted for the current study and for the Key Project papers (Ferrarese et al. 2000b; Freedman et al. 2001). This distance to the LMC appears justified in light of many recent distance measurements (e.g., Carretta et al. 2000), although significant differences certainly remain between techniques and investigators (Udalski et al. 1999; others). A full discussion of the LMC distance issue is beyond the scope of this paper; future adjustments to the LMC distance modulus of 18.50 should be applied as a constant offset to all the distances used herein and to the resulting F160W SBF calibration. The conclusions of this paper are not affected by an uncertainty of 0.15 mag in the LMC distance.

Freedman et al. (2001) also applied an empirical metallicity correction of -0.2 ± 0.2 mag dex⁻¹ in metallicity to the Cepheid calibration such that more metal-rich Cepheids are intrinsically brighter (Freedman et al. 2001; Gibson & Stetson 2001; Kennicutt et al. 1998). For comparison, separate distances for the Key Project galaxies are listed in Table 2 using the new period–luminosity relation alone (“new PL”, Freedman et al. 2001; Gibson & Stetson 2001), and using both the new period–luminosity relation and empirical metallicity correction (“new PL+Z”, Freedman et al. 2001). We chose not to adopt the empirical metallicity correction to the Cepheid distances endorsed by Freedman et al. (2001) because it is not yet entirely clear that the metallicity correction is justified. Udalski et al. (2001) find no evidence for a trend in the luminosity of Cepheids with metallicity. Another study based on theoretical models of Cepheid structure predicts a correction to the period–luminosity relation of +0.27 mag dex⁻¹ in metallicity, which is similar in magnitude but *opposite* in sign from the empirical relation adopted by Freedman et al. (Caputo, Marconi, & Musella 2002). The apparently better agreement with the reliable maser distance to the galaxy NGC 4258 is offered as evidence that the theoretical relationship is more realistic. Of course a slightly smaller distance modulus to the LMC would also explain the difference, so the maser distance to NGC 4258 cannot be regarded as evidence that the metallicity correction must have a particular sign or magnitude. Given the uncertainty in the metallicity correction at this point, we chose not to adjust the *I*-band SBF calibration. In the end, the size of the metallicity correction is not very important provided that the correction is applied consistently through the LMC rung of the distance ladder. We note that the metallicity-corrected Cepheid distances reported by Freedman et al. (2001) are based on Cepheid measurements of LMC Cepheids that have not been corrected for metallicity. Given the similarity in metallicity between Galactic Cepheids and most of the spiral galaxies in which Cepheids have been detected, the effect of a fully-consistent metallicity-corrected Cepheid distance scale and the

uncorrected calibration we adopted for this paper is minimal (approximately 0.02 mag). The data plotted in the figures are based on distances that include no metallicity corrections.

The uncertainties in $\overline{m}_{\text{F160W}}$ were combined in quadrature with the uncertainties in distance modulus to get the final uncertainties in $\overline{M}_{\text{F160W}}$ presented in Table 2. The median uncertainty in $\overline{M}_{\text{F160W}}$ was 0.18 mag for this sample. The estimated systematic error in the Cepheid distance scale, which we incur regardless of which distances are used to compute $\overline{M}_{\text{F160W}}$, is 0.16 mag (Ferrarese et al. 2000a), but could be larger due to blending or other effects (Gibson & Stetson 2001; Mochejska et al. 2000; Ferrarese et al. 2000c). The dominant sources of systematic uncertainty are the distance to the LMC (0.13 mag) and the WFPC2 photometric zero point (0.09 mag). The systematic uncertainty is *not* included in the uncertainty in $\overline{M}_{\text{F160W}}$ listed in Table 2. It is important to note that the uncertainty in $\overline{M}_{\text{F160W}}$ is correlated with the uncertainty in $(V-I)$ for the values derived from I -band SBF distances. $\overline{M}_{\text{F160W}}$ is a function of the I -SBF distance modulus, which is a function of $(V-I)$ color (Tonry et al. 1997).

2.3. Galaxy $(V-I)$ Colors

To calibrate the F160W SBF distance scale, we used the optical $(V-I)_0$ color corrected for extinction to constrain the fluctuation magnitude dependence on stellar population. Most of the $(V-I)_0$ color data in Table 2 were taken from the optical I -band SBF survey (Tonry et al. 2001). Galactic extinction corrections were made using the Schlegel et al. (1998) extinction maps. The data were collected using ground-based telescopes in annular regions that were typically much larger than the central 20-arcsec regions imaged using NIC2. In a few cases we checked the optical colors within the NIC2 field of view to ensure that color gradients within individual galaxies were not significant. For the early-type galaxies in this sample, color gradients do not produce significant color differences between the F160W and I -band regions. A few galaxies, including the spirals not included in the I -band SBF survey (Tonry et al. 2001), were re-observed to allow a direct $(V-I)_0$ color measurement within the NIC2 field of view.

3. Using F160W SBF Magnitudes to Measure Distances

The primary motivation for exploring the variation of $\overline{M}_{\text{F160W}}$ with stellar population was to better calibrate F160W SBFs as a distance indicator. With the high spatial resolution and low background achieved using NICMOS, J2001 demonstrated that fluctuations could

be measured in modest exposures (one or two orbits) to distances beyond 100 Mpc. J2001 utilized a limited subset of the current data set and the Cepheid zero point calibration of Ferrarese et al. (2000b) to empirically calibrate the F160W SBF distance scale. They measured distances to a sample of galaxies reaching redshifts of $10,000 \text{ km s}^{-1}$ for the purpose of determining the Hubble constant. J2001 restricted their calibration to galaxies redder than $(V-I)_0 > 1.16$ and found no significant slope of $\overline{M}_{\text{F160W}}$ with galaxy color.

A constant $\overline{M}_{\text{F160W}}$ calibration is inappropriate for the full color range spanned by the galaxies in this sample (Fig. 1). For the full data set, we fitted a slope adopting the maximum likelihood method described by Liu et al. (2002) to account for the correlated uncertainties in $\overline{M}_{\text{F160W}}$ and $(V-I)$. Uncertainties are correlated because $\overline{M}_{\text{F160W}}$ depends on I -band SBF distances, which are in turn computed using the galaxy $(V-I)$ color. The Liu et al. (2002) method accounts for this non-zero covariance between $\overline{M}_{\text{F160W}}$ and $(V-I)$ in determining the best-fitting slope and intercept. If the covariance were ignored, the slope of the fitted line would be biased (see Liu et al. 2002 for a discussion).

We chose to restrict the sample of galaxies used for calibration purposes to those that show no sign of dust in the NIC2 field of view because clumpy dust makes a galaxy look bumpier, and hence fluctuation magnitudes brighter. Many of the rejected galaxies have well-defined dust lanes that can be masked. The SBF magnitudes are most likely unaffected by the dust, but we exclude them from the calibration fit to be safe. Given the large size of the sample, we can afford to be conservative in excluding dusty galaxies for the purpose of computing the calibration. Fitting the 47 dust-free galaxies gives

$$\overline{M}_{\text{F160W}} = (-4.86 \pm 0.03) + (5.1 \pm 0.5)[(V-I)_0 - 1.16] \quad \text{for } 1.05 < (V-I)_0 < 1.24. \quad (1)$$

The χ^2 per degree of freedom is 1.17, indicating that the uncertainties are reasonable. The slope of $5.1 \pm 0.5 \text{ mag per mag}$ in $(V-I)$ color is steep, and similar to the slope of 4.5 ± 0.25 measured at I -band (Tonry et al. 1997). Liu et al. (2002) found a slope of 3.6 ± 0.8 at K ($2.2 \mu\text{m}$). Stellar population models initially predicted that the slope of IR fluctuation magnitude with color would be opposite that at I -band (Worthey 1994), but it is now clear that a significant slope of the *same* sign persists to $2.5 \mu\text{m}$. The implications of a positive slope are discussed in Section 4.

The relation in Equation 1 is based on I -band SBF distances calibrated using the improved Cepheid period-luminosity relation of Udalski et al. (1999). The Cepheid distances from Freedman et al. (2001) without metallicity corrections were adopted, and we used the same LMC distance modulus of 18.50 mag as Freedman et al. In Figure 1 symbols of three sizes are plotted, with the largest symbols for galaxies with uncertainties less than 0.2 mag and the smallest for measurements with uncertainties greater than 0.3 mag. Median uncertainties in each bin are plotted. Three galaxies in the “dust-free” sub-sample also have

Cepheid variable star distances. They were not included in the fit because they are not independent of the I -band SBF measurements, and their uncertainties arise from different sources. They are, however, plotted in Figure 1 to show that the calibration derived using I -band SBF distances agrees with direct Cepheid distance measurements.

The value of $(V-I)_0 = 1.16$ marks the color at which the strong slope observed in the bluer galaxies makes way to an apparent flattening at the red end. Fits restricted to galaxies with $(V-I)_0 > 1.16$ are consistent with a slope of zero, as found by J2001 using a smaller calibration sample. The sloping fit over the entire color range spanned by the sample, however, is statistically robust. The brightest cluster galaxies observed by J2001 are all redder than $(V-I)_0 = 1.16$, and the use of a constant \overline{M}_{F160W} by J2001 was justified. The stellar population models presented in the following sections suggest that the steep slope shown in Figure 1 cannot continue to arbitrarily red values of $(V-I)$ because galaxies cannot be made of arbitrarily old stars. We therefore adopt the relation between \overline{M}_{F160W} and $(V-I)_0$ given in equation 1 and emphasize that it is *only* applicable to galaxies with $(V-I)$ colors between 1.05 and 1.24.

The small statistical uncertainty in the zero point and the value of χ^2 close to 1 suggests that the “cosmic scatter”, or the variation in \overline{M}_{F160W} not accounted for with the single $(V-I)$ parameter, is small. The calibration presented here suggests that relative distances to galaxies with $(V-I)$ colors typical of elliptical galaxies can be measured with 10% accuracy or better provided that the uncertainty in $(V-I)_0$ is 0.035 mag or smaller, and that the photometric zero point is known to 0.05 mag or better. This estimate of the statistical uncertainty does not include the systematic uncertainty in the distance scale zero point, which includes the uncertainties in the Cepheid distance scale and the distance to the LMC. The scatter increases significantly when dusty galaxies are included. The scatter below the best-fit line in Figure 1 appears larger than above it. This could be caused by the F160W SBF amplitude being under-estimated, or the I -band SBF amplitude being over-estimated (and the distances under-estimated). The uncertainties in the I -band SBF magnitudes are larger than 0.2 mag for most of the outlying points, but there is no obvious sign of a systematic problem with the I -band SBF measurements. The fit has been appropriately weighted by the uncertainties, and is consistent with the most accurate measurements. Excluding them would not significantly change the relation in Equation 1.

J2001 used a constant fluctuation magnitude $\overline{M}_{F160W} = -4.86$ in their determination of the Hubble constant. It is fair to ask what effect the new sloping calibration and revised Cepheid calibration would have if they had been adopted instead. To address this issue, we selected the five galaxies from the J2001 sample that fall within the valid color range $(V-I)_0 < 1.24$ of the current distance calibration and calculated the Hubble constant for the

preferred flow models using exactly the same techniques used by J2001. The increase in the Hubble constant that results from the changes in the zero point and slope of the calibration is not sensitive to the exact flow model adopted or rejection of low- S/N ratio observations (see J2001 for a discussion of these effects). Because the new Cepheid calibration and NIC2 zero point result in a significantly fainter calibration zero point, the value of the Hubble constant would increase by 10% from 76 or 77 to 85 $\text{km s}^{-1} \text{Mpc}^{-1}$. If the new calibration is applied to only the most distant galaxies from J2001, the Hubble constant would increase from 72 $\text{km s}^{-1} \text{Mpc}^{-1}$ to 79. Only a small fraction (1.5% of the 10%) of the change is due to the slope of the calibration; the 0.16 mag change in the Cepheid zero point resulting from the adoption of the improved period-luminosity relation is the dominant factor. If we had adopted the metallicity corrections endorsed by Freedman et al. (2001), the increase in the Hubble constant would have been only 5% (corresponding to a zero point shift of 0.06 mag instead of 0.16 mag). All the changes described happen to affect the calibration in the same direction, i.e., reducing the absolute brightness of the fluctuations and decreasing the implied distances.

4. Stellar Population Models

Infrared SBF magnitudes provide important new constraints on theoretical and semi-empirical stellar population models. The models provide insight into why fluctuation magnitudes vary with color the way they do. Each single-burst, constant-metallicity model is constructed by adopting an initial mass function and uniform composition for an ensemble of theoretical stars. These stars are then allowed to evolve according to the constraints and assumptions of the particular model. At each time step, the luminosity function of the ensemble of stars is integrated to determine observable values, including broad-band colors, line indices, and fluctuation magnitudes. Luminosity fluctuations in a galaxy are proportional to the second moment of the luminosity function (Tonry & Schneider, 1988), and can be computed from the model luminosity function at each time step. Because fluctuations are weighted to the most luminous stars in the population, SBFs provide a way to better measure the contributions of luminous first-ascent red giants and asymptotic giant branch (AGB) stars in unresolved stellar populations.

The first detailed models to successfully predict SBF magnitudes were those of Worthey (1994). SBF predictions from the models of Bruzual & Charlot (Liu et al. 2000, 2002) and Vazdekis (Blakeslee et al. 2001) have recently been published. In this paper, we compare empirical F160W fluctuation magnitudes $\overline{M}_{\text{F160W}}$ to the three sets of models to learn more about the relative ages and metallicities of the galaxies in our sample. These three sets of

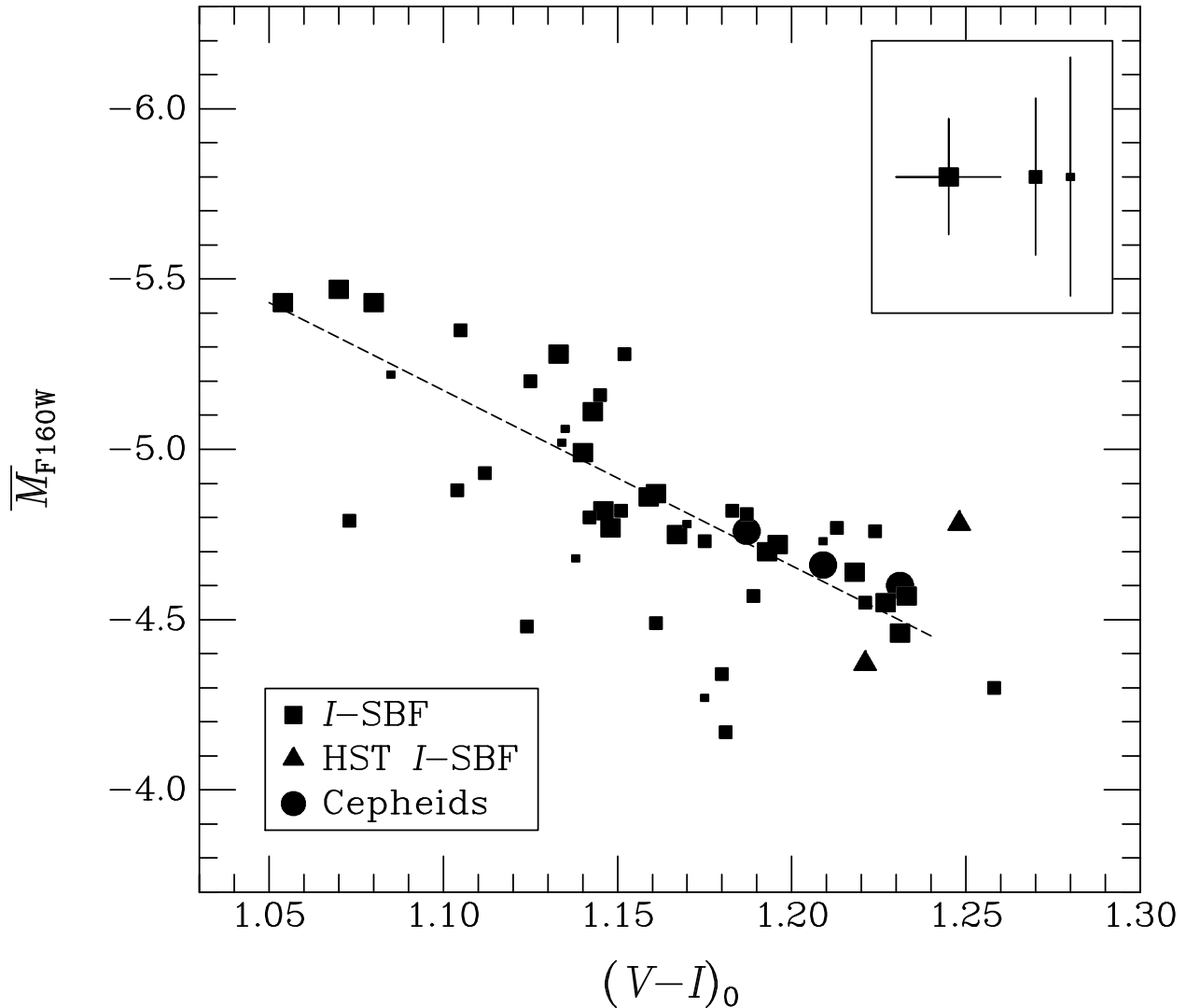


Fig. 1.— Absolute fluctuation magnitudes \overline{M}_{F160W} plotted vs. the extinction-corrected $(V-I)_0$ color for the 47 galaxies that show no signs of dust in the NIC2 field of view. The square points represent \overline{M}_{F160W} values derived using ground-based I -band SBF distances, and the triangles indicate galaxies with I -band SBF distances measured with WFPC2 on the HST. The size of each point indicates the uncertainty in \overline{M}_{F160W} . The largest points have uncertainties less than 0.2 mag, the medium-sized points fall between 0.2 and 0.3 mag, and the smallest points have uncertainties greater than 0.3 mag. Median error bars for each point size are shown at the top of the figure. The circles indicate three galaxies with reliable Cepheid distances (NGC 224=M31, NGC 3031=M81, and NGC 4725). They are also plotted using their I -band SBF distances.

models are the most successful models in common use today for which SBF magnitudes have been published. We also compare the model predictions to the measured fluctuation color ($\overline{m}_I - \overline{m}_{F160W}$), which is independent of the distance measurements. Agreement between observed fluctuation magnitudes and stellar population model predictions can therefore be used to simultaneously confirm the reliability of SBF distance measurements and reinforce the age and metallicity interpretations.

4.1. The Bruzual & Charlot Models

Absolute F160W fluctuation magnitudes are plotted as a function of extinction-corrected $(V-I)_0$ color in the top panel of Figure 2. Data for all 65 galaxies are plotted, including galaxies containing dust that were excluded from the calibration fits. Points for galaxies with Cepheid distances are included as well. In the lower panel of Figure 2 we plotted the fluctuation color ($\overline{m}_I - \overline{m}_{F160W}$) as a function of galaxy $(V-I)$ color. The fluctuation color is independent of distance, and therefore provides additional insight into the stellar populations of the galaxies without being subject to the systematic uncertainties of the distance measurements.

Theoretical fluctuation magnitudes and colors from Liu et al. (2000, 2002) are shown in Figure 2 as dashed (constant age) and dotted (constant metallicity) lines. The Liu et al. (2002) SBF predictions were based on the single-burst population synthesis models of Bruzual & Charlot (1993, 2002), originally described by Liu et al. (2000), and then slightly improved by Liu et al. (2002). The models provide several choices for the input evolutionary tracks and spectral libraries; a detailed comparison of the various options is given by Liu et al. (2000). We use their preferred set of inputs: the Padova evolutionary tracks of Bertelli et al. (1994), semi-empirical spectral energy distributions from Lejeune, Cuisinier, & Buser (1997), and a Salpeter initial mass function.

The Bruzual & Charlot models (Liu et al. 2002) imply that the trend towards brighter fluctuations in bluer galaxies is consistent with younger stellar population models with high metallicities. The redder galaxies appear older and more metal-poor than the bluer ones (model ages are relative to the age of the Universe, thus a model age of 17 Gyr does not imply that a population formed before the Universe was born). A similar trend has been seen in K -band fluctuations (Jensen et al. 1998; Mei, Quinn, & Silva 2001b; Liu et al. 2002). It is interesting to note that there are no fluctuation magnitudes among the bluer galaxies that are consistent with stellar population models older than about 5 Gyr. None of the galaxies appear to have metallicities lower than approximately $[\text{Fe}/\text{H}] = -0.7$. The spread in fluctuation magnitudes with color traces a line of models with nearly constant

metallicity down to $(V-I)_0 = 1.15$; bluer galaxies appear more metal-rich than those with $(V-I)_0 > 1.15$.

The distance-independent plot of fluctuation colors in the lower panel of Figure 2 leads to the same conclusion about the relative ages of galaxies with different colors. The absolute metallicities implied by the $(\overline{m}_I - \overline{m}_{F160W})$ models are very similar to those in the upper panel. The bluer galaxies have the same fluctuation magnitudes as stellar population models with significantly younger ages and slightly higher metallicities than redder galaxies. Agreement between the \overline{M}_{F160W} and the distance-independent $(\overline{m}_I - \overline{m}_{F160W})$ models suggests that the total systematic error in the distance scale calibration is likely to be of order 0.1 mag.

4.2. The Vazdekis Models

In Figure 3 we compare our data to the F160W SBF magnitudes and $(V-I)_0$ colors computed for the Vazdekis models (Blakeslee et al. 2001; Vazdekis 2001). Additional models for populations younger than 4 Gyr were retrieved from http://www.iac.es/galeria/vazdekis/col_lick.html. The Blakeslee et al. models make use of the new Padova isochrones of Girardi et al. (2000), which are transformed to the observable plane using the empirical stellar libraries of Alonso, Arribas, & Martinez-Roger (1996, 1999) and Lejeune et al. (1997, 1998). The Blakeslee et al. (2001) SBF models were computed for the H -filter, so it is necessary to shift the models to F160W. We adopted an empirical correction to the absolute fluctuation magnitudes of

$$\overline{M}_{F160W} = \overline{M}_H + 0.10(\overline{M}_J - \overline{M}_K) \quad (2)$$

based on photometry of red main sequence stars (Stephens et al. 2000). This correction, which is typically 0.17 mag for most models, has the effect of shifting the model lines in Figure 3 down with respect to the points. We also computed the offset between H and F160W by convolving the filter profiles with synthetic spectra of red giant stars (B. Plez, private communication; see also Bessell, Castelli, & Plez 1998). The resulting relation

$$\overline{M}_{F160W} = \overline{M}_H + 0.116(\overline{M}_J - \overline{M}_K) + 0.026 \quad (3)$$

is very close to that derived from the Stephens et al. (2000) data and has no effect on the interpretation, so we adopted the empirical correction in Equation 2.

The top panel in Figure 3 reveals very good agreement between the models as corrected using Equation 2 and the data calibrated using the distances based on the Freedman et al. (2001) Cepheid calibration without metallicity corrections. Uncertainties in the distance calibration are avoided when we compare the fluctuation color $(\overline{m}_I - \overline{m}_{F160W})$ to the models.

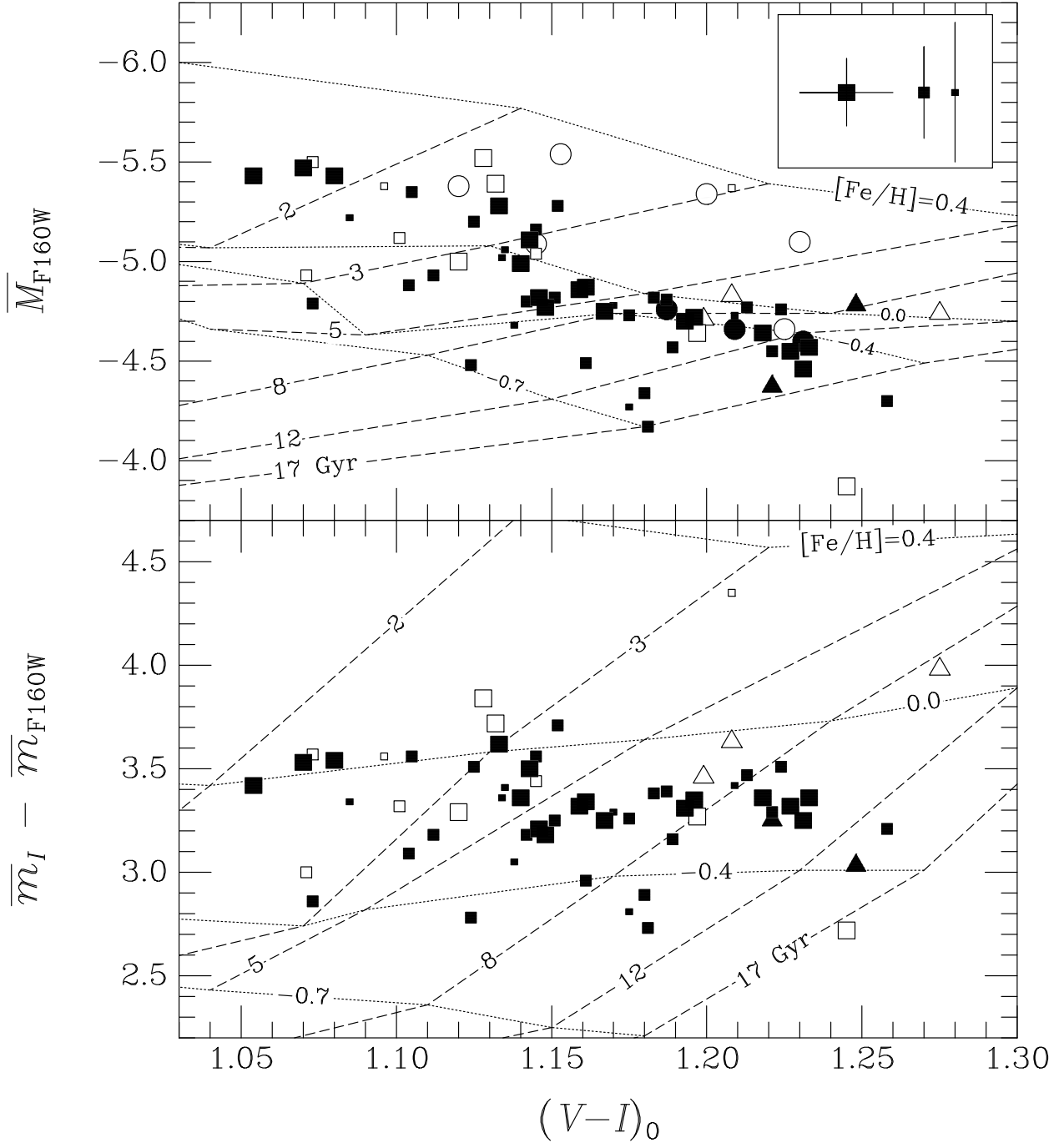


Fig. 2.— The upper panel shows absolute fluctuation magnitudes plotted vs. galaxy optical color. The circular points were calculated using Cepheid distances, the square points using ground-based I -band SBF distances, and the triangles using HST I -band SBF distances. Open symbols indicate galaxies that show signs of dust. Clumpy dust can cause fluctuations to appear brighter. The lines behind the points indicate Liu et al. (2000, 2002) models of constant age (dashed lines) and metallicity (dotted lines). The ages (Gyr) and metallicities ($[\text{Fe}/\text{H}]$) of the models are indicated. The lower panel shows the distance-independent fluctuation color as a function of $(V-I)_0$.

The ages and metallicities implied by the $(\overline{m}_I - \overline{m}_{F160W})$ models are in very good agreement with those of the \overline{M}_{F160W} models and with the Liu et al. (2002) models. Once again, a change in the distance scale zero point of more than approximately 0.1 mag would compromise the compatibility between the models.

The Vazdekis models show a compression in \overline{M}_{F160W} of the higher-metallicity and younger-age tracks compared to the Liu et al. (2000, 2002) models. This is partly due to the fact that the maximum metallicity shown for the Blakeslee et al. (2001) models is 0.2, while that of Liu et al. is 0.4. It is also partly due to the difference in slope between the youngest populations. While there are many differences in the details of the Vazdekis and Bruzual & Charlot models, the choice of isochrones is perhaps the most significant for the current study. If we apply the newer evolutionary tracks (Girardi et al. 2000) adopted by Blakeslee et al. (2001) to the Bruzual & Charlot models (Liu et al. 2000, 2002), we find that the resulting age tracks are nearly horizontal and lie midway between the two sets of models shown in Figures 2 and 3.

4.3. The Worthey Models

Figure 4 shows the F160W data plotted with the Worthey (1994) models. Worthey models are currently available via the web at http://astro.wsu.edu/worthey/dial/dial_a_model.html. F160W models were constructed by convolving the basic “vanilla” model spectral energy distributions at each age and metallicity with the filter profile of the NIC2 F160W filter (G. Worthey, private communication). The default Worthey models use a Salpeter initial mass function and a helium fraction of $Y = 0.228 + 2.7Z$. There are differences in detail between the Worthey models and those presented in the previous sections. In particular, the Worthey models imply older ages for galaxies of a given color, and unreasonably large ages for the reddest galaxies. Note that the calibration changes to the Freedman et al. (2001) Cepheid zero point without metallicity corrections makes the comparisons to the Worthey \overline{M}_{F160W} models worse than they would have been using the previous Key Project calibration (Ferrarese et al. 2002b, J2001). The comparison of the distance-independent $(\overline{m}_I - \overline{m}_{F160W})$ models to the data yields ages and metallicities in excellent agreement with the conclusions of the previously-considered models. The redder galaxies have slightly sub-solar metallicities and old ages, while the bluer galaxies appear to have higher metallicities and significantly younger ages. It appears that the Worthey (1994) models may have an offset in absolute magnitude, but the relative brightnesses of the models at different wavelengths are reliable.

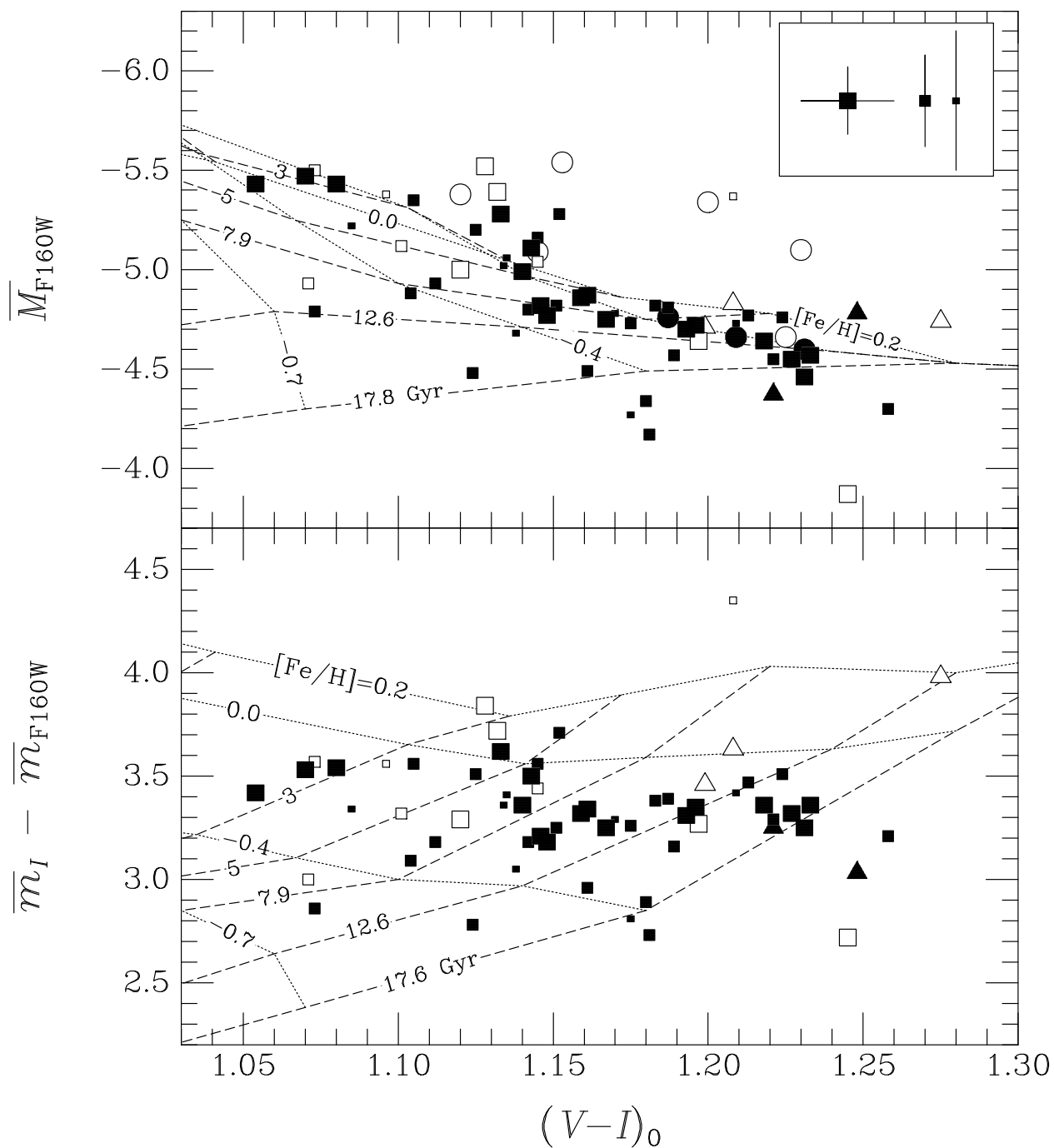


Fig. 3.— Absolute fluctuation magnitudes and fluctuation colors plotted with the Vazdekis stellar population models (Blakeslee et al. 2001), translated to the F160W filter as described in the text. The symbols are the same as in Figure 2.

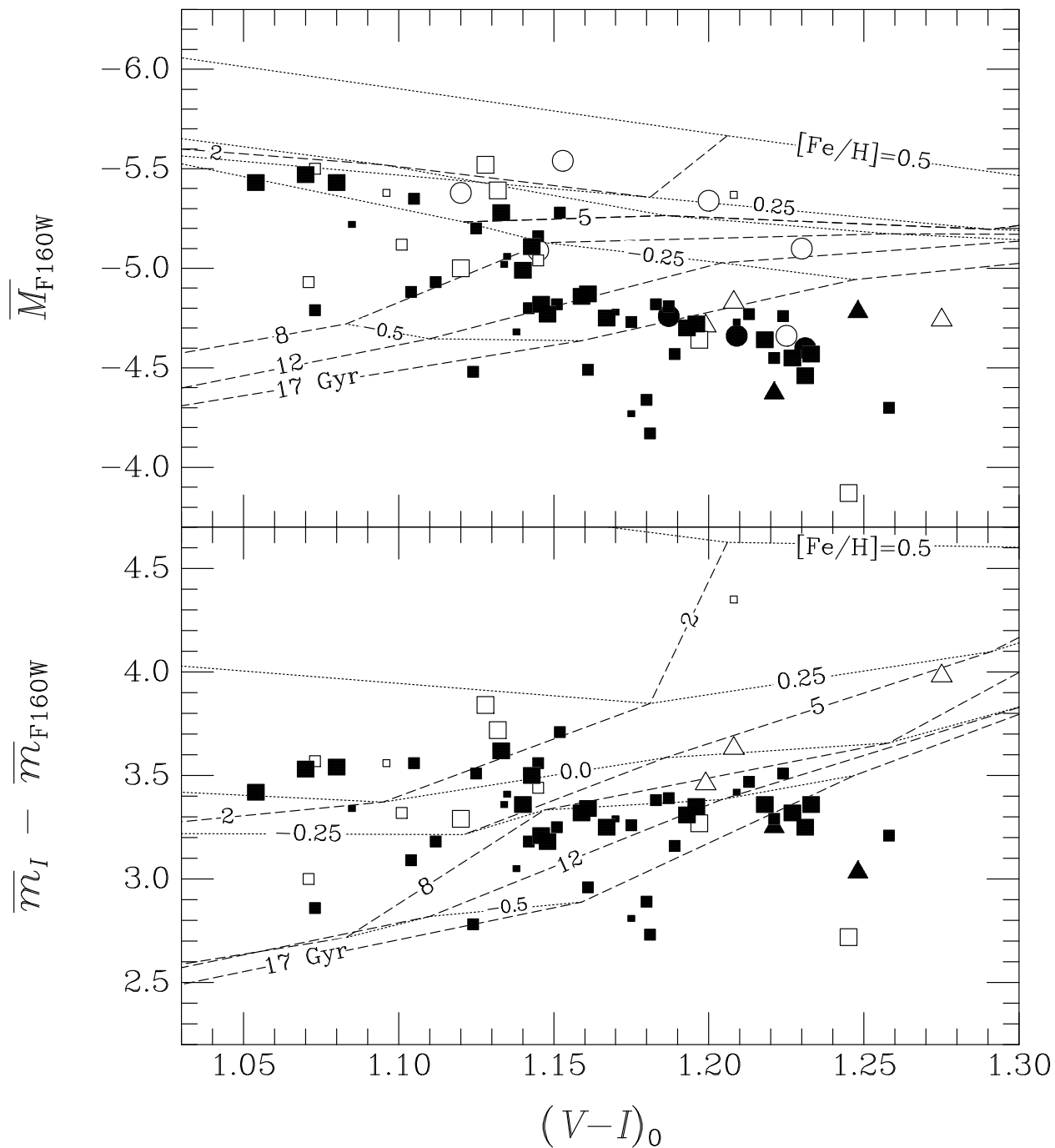


Fig. 4.— Absolute fluctuation magnitudes and fluctuation colors plotted with the Worthey (1994) models. The symbol definitions and uncertainties are the same as in Figure 2. Note that the triangular gap on the left is caused by the lack of published models for young, metal-poor populations, and is not a feature of the models.

4.4. Composite Stellar Population Models

Fluctuation magnitudes are dominated by the youngest stars in a population. Statistically, measured SBFs are the ratio of the second moment of the stellar luminosity function to the first, and therefore are very sensitive to the brightest stars. When comparison of SBF magnitudes to the models suggests the presence of young or intermediate-age populations (<5 Gyr), only a fraction of the stars would have to be young for the fluctuation amplitude to be high; the majority of the stars may be much older.

Tonry, Ajhar, & Luppino (1990) were the first to attempt to use composite stellar population models to explain optical SBF observations, but the inadequacy of their model isochrones and colors led Worthey (1993) to question the validity of their results. More recently, Blakeslee et al. (2001) and Liu et al. (2002) have compared composite stellar population models to observational SBF data. Blakeslee et al. found that a 3-component model that includes a $\sim 10\%$ metal-poor component reproduces the observed *I*-band SBF slope and agrees with the IR SBF results presented here.

In Figure 5 we compare our fluctuation magnitudes to the composite stellar population models of Liu et al. (2002) re-calculated for the F160W filter. In the three scenarios shown in Figure 5, 20% of the final mass formed six Gyr after the principal population. Composite populations with smaller mass fractions and smaller age differences would fall between the tracks shown in Figure 5; these models are meant to be representative and are shown for comparison with those published by Liu et al. (2002). The total time since formation is indicated in Figure 5 on each evolutionary track, thus the 7 Gyr point marks the magnitude and color of a population where 80% of the stars by mass are 7 Gyr old and the other 20% formed 1 Gyr ago. The top line is for a burst with higher metallicity ($[\text{Fe}/\text{H}] = +0.4$) than the original solar-metallicity population. The middle track is for a burst population of solar metallicity, and the lowest track is for a burst with lower-than-solar metallicity ($[\text{Fe}/\text{H}] = -0.7$). In all three cases the majority of the stars (80% of the final mass) formed from solar-metallicity gas.

Figure 5 shows that the bright fluctuations in bluer galaxies may be the result of a recent burst of star formation within the last ~ 2 Gyr with a total mass fraction of $\sim 20\%$. Liu et al. (2002) came to the same conclusion comparing *K*-band SBF data to the composite models. The F160W data in Figure 5 suggest that the burst took place in previously-enriched gas. If recent episodes of star formation are triggered by mergers with dwarf galaxies with lower than solar metallicity, the star formation must take place in gas previously enriched in the larger galaxy. Figure 5 suggests that as time goes on, bursts of star formation take place in increasingly metal-rich gas.

The bottom panel of Figure 5 shows the comparison of fluctuation color ($\overline{m}_I - \overline{m}_{F160W}$) to the composite models. The ($\overline{m}_I - \overline{m}_{F160W}$) models imply slightly lower absolute metallicities for galaxies at the blue end of the color distribution than the \overline{M}_{F160W} models do. None of the points in the lower panel fall much above the solar metallicity ($\overline{m}_I - \overline{m}_{F160W}$) track, in contrast to the data in the top panel. The metallicities implied for the redder galaxies are the same in both panels. The metallicities implied by the ($\overline{m}_I - \overline{m}_{F160W}$) models support the conclusion that more-recent star formation takes place in progressively higher-metallicity gas.

4.5. Comparing Fluctuations to the $H\beta$ Index

The well-known age-metallicity degeneracy makes it difficult to use broad-band optical colors to distinguish old, metal-poor populations from younger, metal-rich ones (e.g., Worthey 1994). One currently popular technique for determining ages and metallicities, particularly in young populations ($t < 5$ Gyr), is to compare the age-sensitive $H\beta$ absorption line strength to a metal line that is sensitive to metallicity. IR SBFs also break the age-metallicity degeneracy and allow one to distinguish young, blue populations from older, metal-poor populations (Liu et al. 2000; Blakeslee et al. 2001). SBFs are dominated by the brightest stars in a galaxy, which in relatively young and intermediate-age populations ($1 < t < 5$ Gyr) are evolved red giant and AGB stars. The populations we are considering are not actively forming stars, and are not so young as to contain massive luminous OB stars or emission nebulae. In contrast to SBFs, the $H\beta$ absorption arises from main sequence stars near the main sequence turn-off. Because $H\beta$ and SBF measurements arise from *completely different* groups of stars, and are measured using *completely different* techniques, the F160W SBF measurements presented here provide an important independent confirmation that $H\beta$ absorption is truly revealing differences in the ages of stellar populations. F160W fluctuation magnitudes and $H\beta$ absorption are both sensitive probes of young stellar populations. The fact that the two techniques agree for individual galaxies in this sample is significant.

In Figure 6 we compare the age-sensitive \overline{M}_{F160W} to $H\beta$ and use the Bruzual & Charlot models of Liu et al. (2002) to infer relative ages and metallicities. We collected high-quality $H\beta$ measurements on the Lick/IDS system from three recent studies (Kuntschner et al. 2000; Kuntschner 2000; Trager et al. 2000). These measurements include a sample of 14 galaxies in the Fornax cluster and 10 others, including some in the Local Group, Virgo, Leo clusters. The three studies measured $H\beta$ values in apertures of different sizes. Kuntschner (2000) used a single aperture size for the Fornax cluster galaxies. Kuntschner et al. (2000) scaled their measurements by distance to a common physical scale. The Trager et al. (2000) data

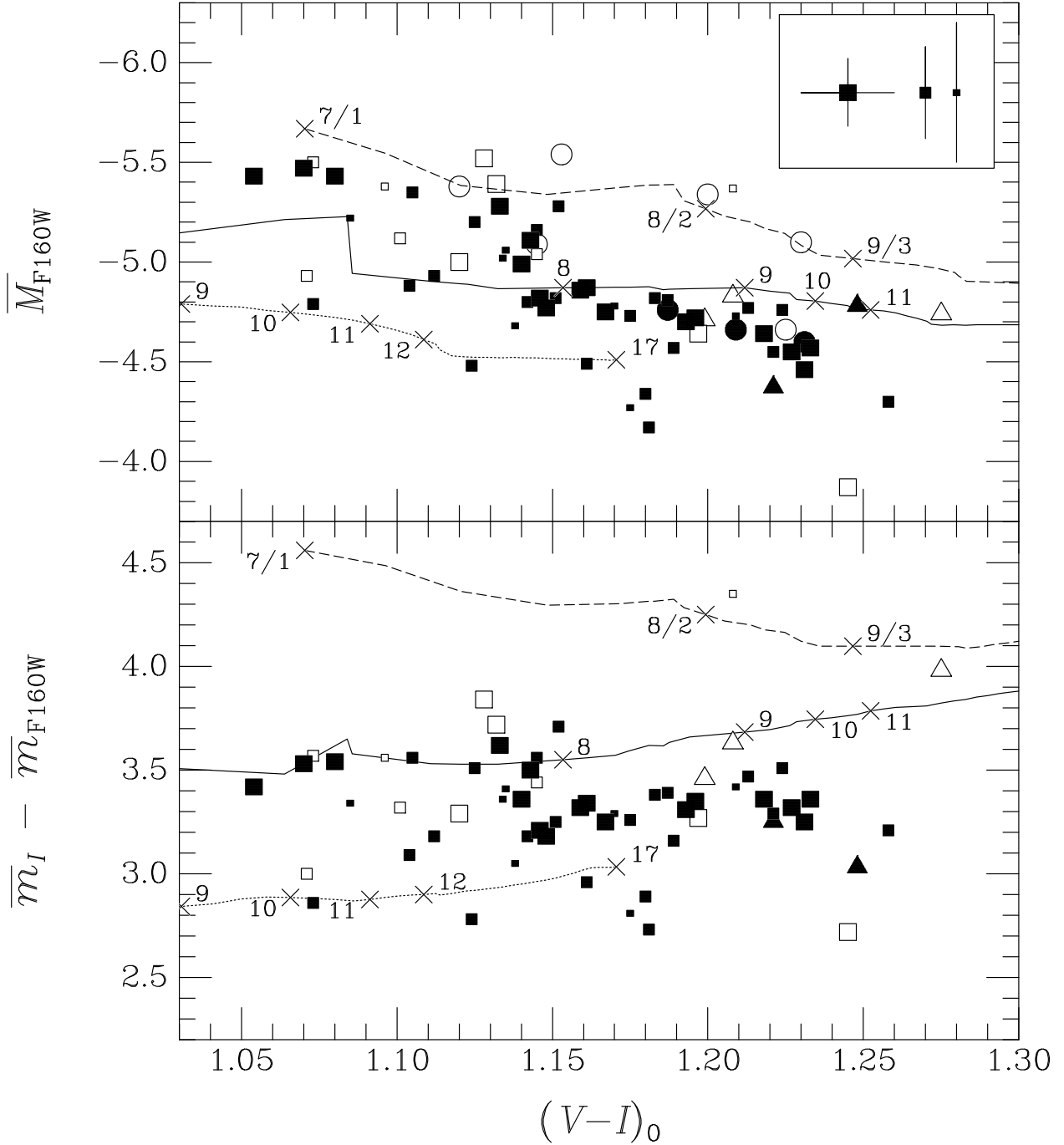


Fig. 5.— Three composite stellar population models (Liu et al. 2002) compared to the SBF measurements. In each case, the model population is composed of two bursts separated by 6 Gyr, with the younger population containing 20% of the total mass. The total age of the composite population in Gyr is indicated by the numbers: 8 indicates the position on the line of a population where 80% of the stars by mass formed 8 Gyr ago and 20% formed 2 Gyr ago. The top (dashed) line indicates models with the second burst forming from super-solar metallicity gas ($[Fe/H] = 0.4$), the center (solid) line from solar metallicity gas ($[Fe/H] = 0.0$), and the lowest line (dotted) from sub-solar metallicity gas ($[Fe/H] = -0.7$). In all cases the older population is of solar metallicity.

are measured in an aperture scaled to the size of the galaxy ($r_e/8$). It is unnecessary to adjust the measurements to a common system since Kuntschner et al. (2000) found that $H\beta$ does not change significantly with radius from the galaxy center. The Kuntschner and Trager studies apply a slightly different correction for $H\beta$ emission; we applied a small correction of 0.1 times $[OIII]\lambda 5007$ to the Trager et al. data to match the correction used in the Kuntschner papers. The $H\beta$ measurements are listed in Table 1. Two galaxies were measured by both teams: $H\beta$ measurements for NGC 3379 are presented in all three papers, and data for NGC 4472 are published in two. The $H\beta$ values listed in Table 1 are averages of all measurements, and the uncertainties were added in quadrature. The standard deviation of the different measurements was less than or equal to the total uncertainties in both cases.

The trend seen in Figure 6 shows that the galaxies span a wide range in age, both as determined using $H\beta$ and \overline{M}_{F160W} . There is clearly a correlation between \overline{M}_{F160W} and $H\beta$. The stellar population models (Liu et al. 2002) have lines of constant age perpendicular to the correlation between \overline{M}_{F160W} and $H\beta$ seen in Figure 6, indicating that both are sensitive to young and intermediate-age populations (even though they sense very different *components* of the young populations). The fact that both techniques lead to the same conclusion that early-type galaxies often contain young stellar populations strengthens the conclusion considerably. The stellar population models become somewhat more compressed for ages greater than 8 Gyr, when the A stars responsible for $H\beta$ absorption have evolved off the main sequence, and the red giant and AGB stars responsible for the fluctuations are intrinsically fainter and more uniform in brightness (the model ages are best interpreted in a relative sense; observations that agree with the oldest models do not imply ages older than the Universe).

The absolute metallicities implied by Figure 6 are only marginally higher than those seen in the previous comparisons, and the trend with age is consistent. In the lower panel of Figure 6 the $H\beta$ values are compared to the fluctuation color ($\overline{m}_I - \overline{m}_{F160W}$), which is distance independent. The \overline{M}_{F160W} and ($\overline{m}_I - \overline{m}_{F160W}$) models disagree slightly. The fluctuation color models suggest somewhat lower metallicities than the \overline{M}_{F160W} models, in agreement with the other model comparisons.

Both panels in Figure 6 show a relationship between IR fluctuations and $H\beta$. The models suggest that both elliptical and S0 galaxies span a very wide range in age and a relatively narrow range of metallicity. This result disagrees somewhat with the conclusion of Kuntschner (2000), who found that only the S0 galaxies in Fornax have a wide spread in age. Kuntschner’s limited sample of Fornax ellipticals appear uniformly old and span a range in metallicity. Our results are consistent with the conclusions of Trager et al. (2000), who found a wide age spread among a sample of ellipticals drawn from a variety of environments.

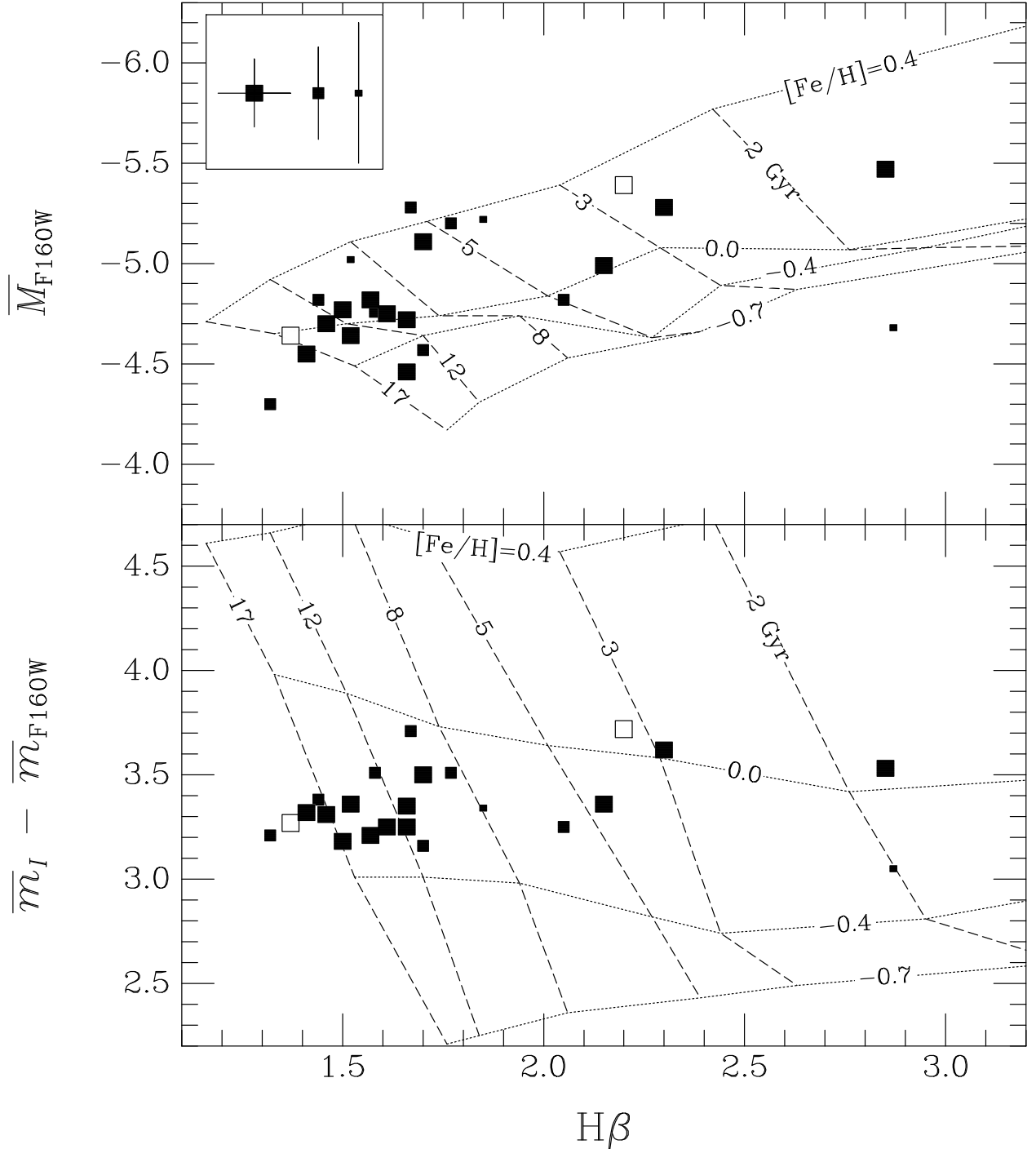


Fig. 6.— Absolute fluctuation magnitudes and fluctuation colors plotted vs. the $H\beta$ absorption line index (in \AA) for a subset of 24 galaxies (Kuntschner et al. 2000, and Kuntschner 2000, and Trager et al. 2000). The majority of the galaxies are ellipticals in the Fornax cluster (see Table 1). $H\beta$, like \overline{M}_{F160W} , is sensitive to the age of the stellar population. Model predictions of both \overline{M}_{F160W} and $H\beta$ are shown for the Liu et al. (2000, 2002) models, with ages and metallicities indicated. The symbol definitions are the same as in Figure 2.

4.6. Common Ground

In detail, there are significant differences between the different models in predicted fluctuation magnitudes. Differences have also been noted at other wavelengths (Blakeslee et al. 2001, Liu et al. 2002, Mei et al. 2001b). In general, however, the comparison of empirical fluctuation magnitudes to the models yields a broadly consistent picture. Fluctuation amplitudes in galaxies redder than $(V-I)_0 > 1.16$ are all consistent with stellar populations older than approximately 8 Gyr and of slightly sub-solar metallicity. Galaxies on the bluer end of the color range all appear consistent with the youngest (2 to 5 Gyr) models in both absolute fluctuation magnitude and fluctuation color. Regardless of which model is considered, these blue, lower-luminosity galaxies appear to be more metal-rich than the redder ellipticals. None of the bluer galaxies in this sample have fluctuation magnitudes that are consistent with old (>5 Gyr) single-burst stellar population models with low metallicities. The majority of stars in the blue galaxies may still be old, as the fluctuation magnitudes are dominated by young stars in a population. Composite stellar population models reinforce the conclusions of the single-age stellar population models.

The conclusion that bluer early-type galaxies are younger and more metal-rich seems to contradict the observed relationship between mass and metallicity in giant ellipticals where less massive (bluer) systems retain less enriched gas, and should therefore have lower metallicities than the massive ellipticals. The SBF magnitudes are dominated by the brightest and youngest stars in a galaxy, however, so our conclusion regarding metallicity may be consistent with the mass–metallicity relation if the bluer ellipticals have lower metallicities overall and some small fraction of their stars formed relatively recently from more metal-rich gas. The uncertainty in the assumed luminosity evolution of the AGB stars in the youngest population models also serves to minimize the importance of the apparent contradiction. A modest excess in the real AGB population over the models would result in enhanced SBF magnitudes that would appear the same as enhanced metallicities.

The differences between models indicate that the details of the evolutionary tracks that are used in the models deserve further attention. Furthermore, the Padova evolutionary tracks are not computed beyond the onset of the thermally-pulsating stage of the AGB, and the modelers have employed a synthetic parameterization of the evolution of AGB stars to attempt to reproduce the luminosity function of realistic populations. The data presented here can provide feedback that should result in improved understanding of the luminosities and lifetimes of luminous AGB stars. It is also clear that real galaxies are not composed of coeval populations of stars of constant metallicity.

The excellent agreement between the data and the models for both the \overline{M}_{F160W} and the distance-independent $(\overline{m}_I - \overline{m}_{F160W})$ models suggests that the Cepheid distances are

probably reliable to better than 10%. For the current study we adopted the new Cepheid period-luminosity relations of Udalski et al. (1999), no metallicity corrections, and a distance modulus to the LMC of 18.50 mag.

5. Galaxy Morphologies and SBF Magnitudes

Figure 7 shows the absolute fluctuation magnitudes separated into bins by morphological type. Galaxy morphology classifications were taken from de Vaucouleurs et al. (1991, RC3). Absolute fluctuation magnitudes and the projected ellipticities of the galaxies on the sky are plotted in Figure 8 (RC3). The shapes of the symbols in Figure 8 are the same as the optical shapes of the galaxies measured well outside the NICMOS field of view. Morphological types and ellipticities from RC3 are listed in Table 1.

As a group, lenticular S0 galaxies are bluer than the elliptical population; nevertheless, the overlap between elliptical and S0 galaxies covers almost the entire range in color covered by this sample. The bulges of spiral galaxies also span the full range of color and \overline{M}_{F160W} spanned by the elliptical galaxies. Some dusty spiral bulges have fluctuation magnitudes that are significantly brighter than the early-type galaxies of the same color, most likely because the fluctuation amplitude is enhanced by the presence of clumpy dust. Some galaxies of all types included in our sample ($T = -6$ to $+4$) apparently contain bluer and brighter intermediate-age populations near their centers. While most of the galaxies are found in clusters or groups, the sample covers a range of environment from dense, compact clusters like Fornax, to lower-density groups and clusters (Leo, Virgo, and Ursa Major). Thirteen galaxies are not associated with any obvious group or cluster (as defined by Faber et al. 1989).

6. Summary

1. Using F160W SBF magnitudes to accurately determine extragalactic distances requires that the color of the galaxy be known. The best calibration fit is given in Equation 1. To achieve an accuracy of $\sim 10\%$ or better, the uncertainty in $(V-I)_0$ color should be less than ~ 0.035 mag. Applying the new calibration to the distant F160W SBF data of J2001 would result in a value of the Hubble constant that is 10% larger than that published previously; almost all of the difference (8%) is due to the improved Cepheid period-luminosity relation of Udalski et al. (1999).

2. The reddest, most-massive ellipticals appear older (when compared to theoretical

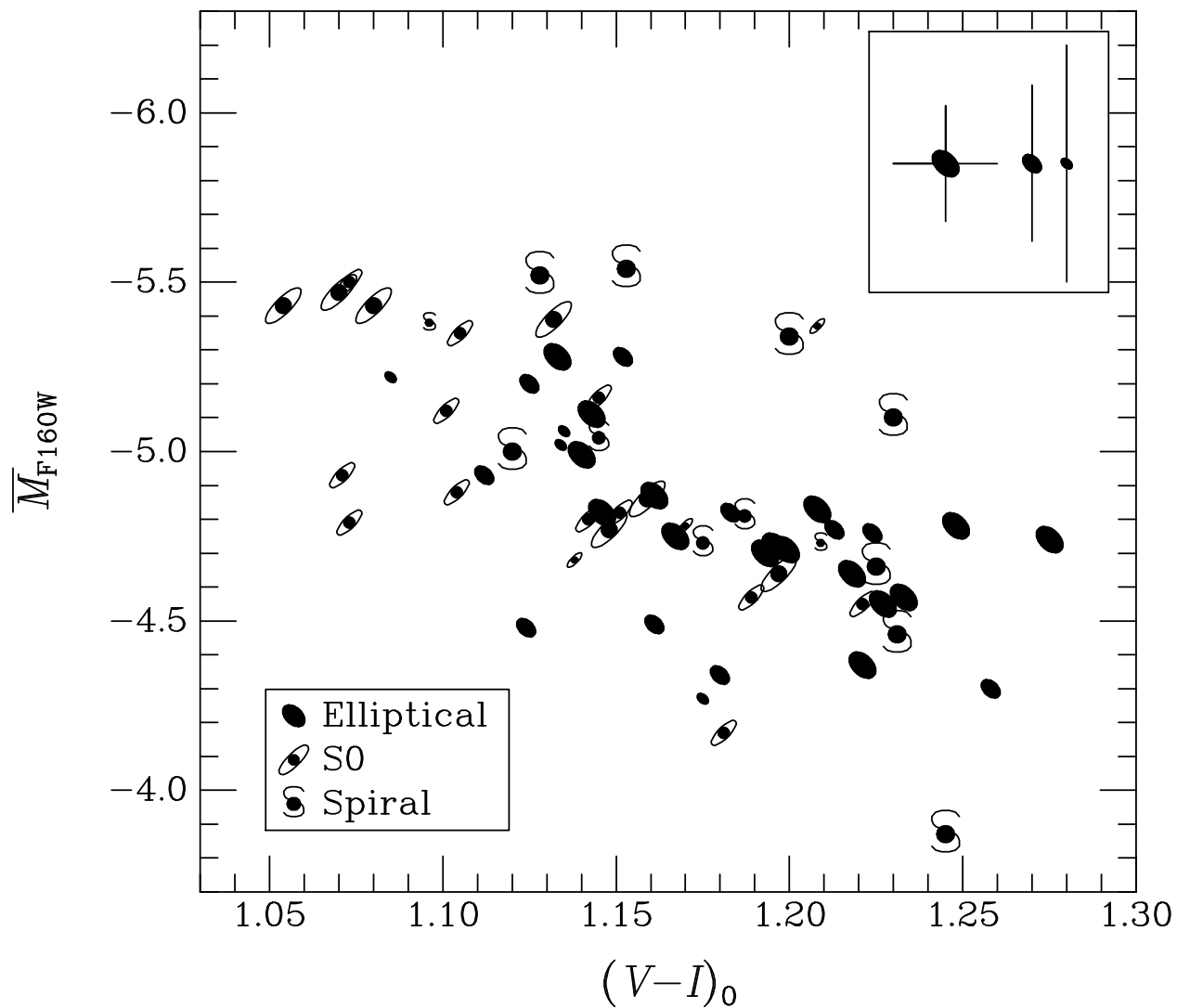


Fig. 7.— Absolute fluctuation magnitudes plotted vs. color by galaxy type. T-types (RC3) of -4 to -6 are plotted as ellipticals, -3 , -2 , and -1 as lenticular (S0) galaxies, and types $T \geq 0$ are shown as spirals. As in the previous figures, the largest symbols have the smallest uncertainties (median uncertainties are indicated in the upper right corner).

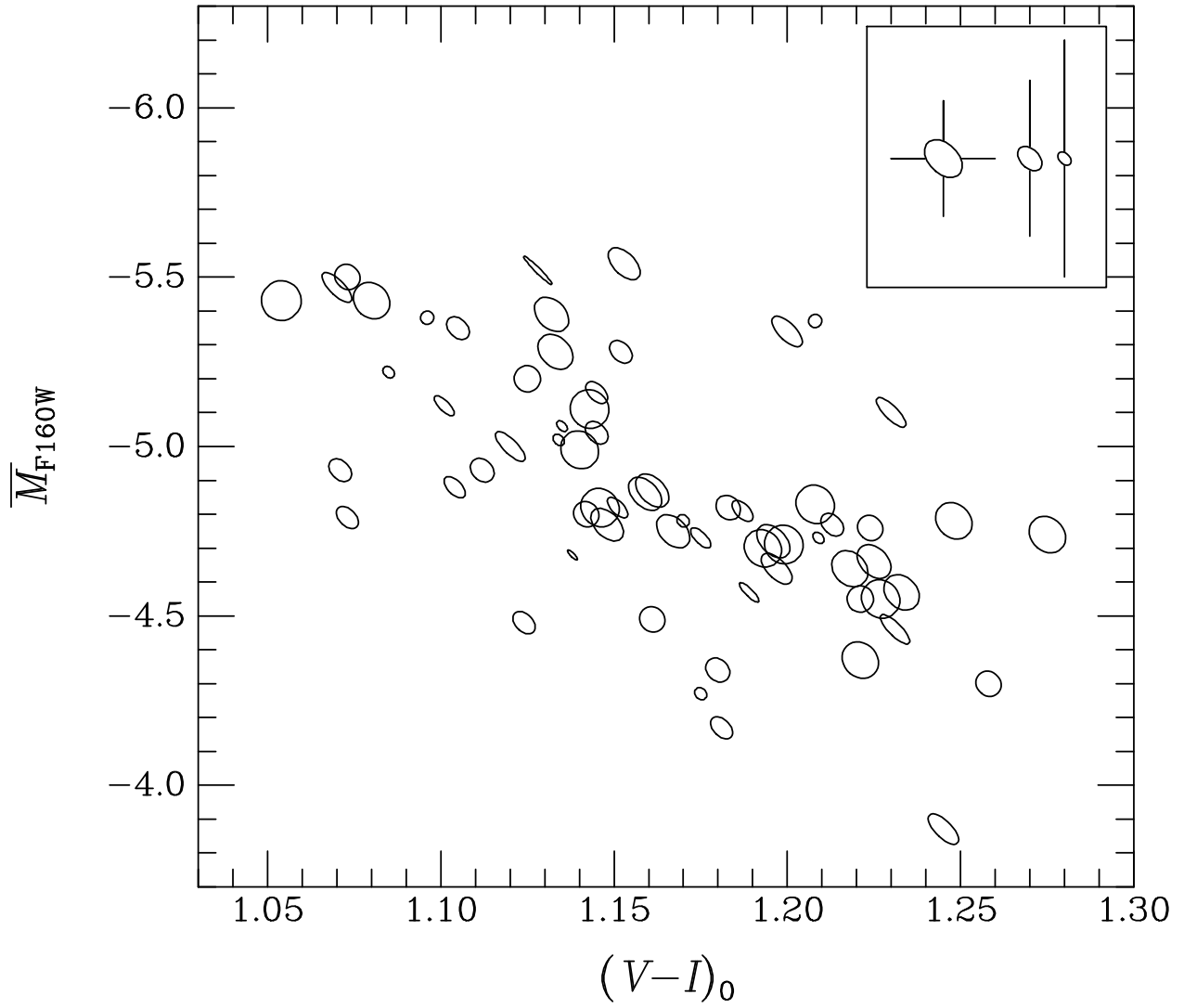


Fig. 8.— Absolute fluctuation magnitudes plotted vs. color, with symbol shapes that indicate the projected ellipticity on the sky (RC3).

stellar population models) than the less-luminous bluer galaxies. There are *no* galaxies in the blue half of our sample that have fainter fluctuation magnitudes consistent with very low metallicity ($[\text{Fe}/\text{H}] < -0.7$) and old age ($t > 5$ Gyr) stellar population models. Comparison with stellar population models suggests that the youngest galaxies have somewhat higher metallicities than the older ellipticals. None of the galaxies have fluctuation magnitudes that are too bright to be accommodated by the young, metal-rich models.

3. Composite stellar population models composed of $\sim 20\%$ younger stars by mass are also consistent with the brighter fluctuation magnitudes in bluer galaxies, provided the younger stars formed from gas of equal or higher metallicity than the gas that formed the older stellar population.

4. The $H\beta$ line index and fluctuation magnitude $\overline{M}_{\text{F160W}}$ are both sensitive to young and intermediate-age stellar populations with ages between one and a few Gyr. Age estimates from the two techniques are consistent. The agreement is significant because the two types of measurements make use of *completely different* techniques and are sensitive to *different populations* of stars.

5. Comparison of fluctuation magnitudes and distance-independent fluctuation colors to the predictions of stellar population models provides an independent check on the distance scale calibration. If the models are correct, at least in the relative brightnesses between the I and F160W bands, then the total systematic error in the Cepheid distance scale is possibly $\lesssim 0.1$ mag.

6. The S0 galaxies and dust-free spiral bulges in this sample have fluctuation magnitudes that are indistinguishable from those of the elliptical galaxies of the same color. Young and intermediate-age populations of relatively high metallicity must therefore be present in all galaxy types on the blue end of the color distribution. While there is a greater fraction of S0 galaxies among the bluer galaxies, galaxies of all types are found across the entire color range.

This study benefited greatly from NICMOS data collected as part of several programs, and we thank those who worked to acquire that data. In particular, we are grateful to those who helped ensure that the data would be appropriate for SBF analysis and assisted with the data reductions (D. Geisler, J. Elias, J. R. Graham, and S. Charlot). We greatly appreciated the helpful comments of L. Ferrarese, T. Lauer, M. Postman, and R. Weymann. This study made use of data collected by the Optical SBF team (J. Tonry, J. Blakeslee, E. Ajhar, and A. Dressler), and we thank them for providing color photometry and I -band SBF data. Finally, we wish to thank S. Charlot, A. Vazdekis, and G. Worthey for constructing the SBF stellar population models.

This research was supported in part by NASA grant GO-07453.0196A. The NICMOS GTO team was supported by NASA grant NAG 5-3042. J. Jensen acknowledges the support of the Gemini Observatory, which is operated by the Association of Universities for Research in Astronomy, Inc., on behalf of the international Gemini partnership of Argentina, Australia, Brazil, Canada, Chile, the United Kingdom, and the United States of America. M. Liu acknowledges the support of a Beatrice Watson Parrent Fellowship.

Table 1. F160W NIC2 Observational Data

Galaxy	Grp. ^a	Prog. ID	Obs. dataset	Position (J2000)		t_{exp} (s)	A_B ^b (mag)	cz (km s ⁻¹)	T ^c	e ^c	H β ^d (Å)
				RA	dec						
NGC 7814	...	7330	N3ZB1A	00:03:15.12	16:08:49.7	640	0.194	1054	+2	0.58	...
NGC 221	282	7171	N4EY01	00:42:41.85	40:51:51.8	64	0.268	-145	-6	0.26	2.30±0.05
NGC 224	282	7171	N4EYA1	00:42:44.33	41:16:08.4	64	0.268	-300	+3	0.68	1.66±0.07
NGC 404	282	7330	N3ZB2L	01:09:26.80	35:43:05.3	640	0.253	-48	-3	0.00	...
NGC 524	...	7886	N4RW05	01:24:47.74	09:32:19.8	640	0.357	2421	-1	0.00	...
NGC 708	27	7453	N4HD14	01:52:46.49	36:09:06.5	960	0.379	4871	-5	0.17	...
NGC 821	...	7886	N4RW27	02:08:21.15	10:59:42.0	640	0.478	1718	-5	0.37	1.66±0.04
NGC 1052	207	7886	N4RW09	02:41:04.75	-08:15:20.7	640	0.115	1507	-5	0.31	...
NGC 1172	29	7886	N4RW10	03:01:36.04	-14:50:12.0	640	0.290	1550	-4	0.22	...
NGC 1316	31	7458	N4B707	03:22:41.51	-37:12:33.0	768	0.090	1760	-2	0.29	2.20±0.07
NGC 1351	31	7886	N4RW15	03:30:35.01	-35:51:14.2	640	0.061	1518	-3	0.40	1.50±0.10
NGC 1339	31	7458	N4B710	03:28:06.58	-32:17:04.3	256	0.057	1392	-4	0.28	1.52±0.11
NGC 1344	31	7458	N4B709	03:28:18.98	-31:04:04.3	256	0.077	1169	-5	0.42	...
NGC 1365	(31)	7330	N3ZB30	03:33:35.36	-36:08:22.2	640	0.088	1662	+3	0.45	...
NGC 1373	31	7458	N4B7A3	03:34:59.25	-35:10:17.0	256	0.060	1334	-4	0.26	1.85±0.10
NGC 1374	31	7458	N4B703	03:35:16.66	-35:13:34.3	256	0.060	1294	-5	0.07	1.57±0.09
NGC 1375	31	7458	N4B706	03:35:16.84	-35:15:56.5	256	0.063	740	-2	0.62	2.85±0.09
NGC 1379	31	7453	N4HD07	03:36:04.03	-35:26:26.8	384	0.052	1324	-5	0.05	1.70±0.09
NGC 1380	31	7458	N4B702	03:36:27.15	-34:58:33.4	265	0.075	1877	-2	0.52	1.37±0.11
NGC 1381	31	7458	N4B7A6	03:36:31.90	-35:17:46.4	256	0.058	1724	-2	0.72	1.70±0.06
NGC 1386	31	7458	N4B708	03:36:45.37	-35:59:57.0	256	0.054	868	-1	0.62	...
NGC 1380A	31	7453	N4HDA7	03:36:47.62	-34:44:25.2	384	0.063	1561	-2	0.71	2.87±0.13
NGC 1387	31	7458	N4B701	03:36:57.06	-35:30:22.7	256	0.055	1302	-3	0.00	...
NGC 1389	31	7458	N5B7A8	03:37:11.68	-35:44:45.5	256	0.046	986	-3	0.40	...
NGC 1399	31	7453	N4HD09	03:38:29.09	-35:27:00.6	384	0.058	1425	-5	0.07	1.41±0.08
NGC 1404	31	7453	N4HDA9	03:38:52.04	-35:35:38.3	384	0.049	1947	-5	0.11	1.58±0.08
NGC 1400	32	7886	N4RW17	03:39:30.81	-18:41:16.1	640	0.280	558	-3	0.13	...
NGC 1427	31	7458	N4B704	03:42:19.48	-35:23:33.8	256	0.048	1388	-4	0.32	1.67±0.05
NGC 1426	32	7886	N4RW18	03:42:49.09	-22:06:29.2	640	0.070	1422	-5	0.37	...
IC 2006	31	7458	N4B705	03:54:28.53	-35:57:54.8	256	0.048	1364	-5	0.15	1.44±0.10
NGC 1553	211	7886	N4RW21	04:16:10.28	-25:46:50.8	640	0.065	1080	-2	0.37	...
NGC 3032	...	7330	N3ZB82	09:52:08.03	29:14:08.3	640	0.072	1533	-2	0.11	...
NGC 3056	...	7886	N4RW29	09:54:32.79	-28:17:53.0	640	0.386	1017	-1	0.37	...
NGC 3031	...	7331	N3ZD0N	09:55:32.70	69:03:54.0	384	0.347	-34	+2	0.48	...
NGC 3351	(57)	7330	N3ZB1I	10:43:58.08	11:42:16.6	640	0.120	778	+3	0.32	...
NGC 3368	57	7330	N3ZB2N	10:46:45.87	11:49:13.6	640	0.109	897	+2	0.31	...
NGC 3379	57	7453	N4HD01	10:47:49.56	12:34:53.0	384	0.105	920	-5	0.11	1.46±0.16
NGC 3384	57	7453	N4HDA1	10:48:16.88	12:37:44.2	384	0.115	735	-3	0.54	2.05±0.11
NGC 3928	155	7331	N3ZD0A	11:51:47.70	48:41:01.8	256	0.084	982	+3	0.00	...
NGC 4143	155	7330	N3ZB95	12:09:36.10	42:32:01.2	640	0.055	784	-2	0.37	...
NGC 4150	55	7886	N4RW39	12:10:33.69	30:24:06.0	640	0.078	244	-2	0.31	...
NGC 4261	150	7868	N4RV02	12:19:23.22	05:49:31.0	192	0.076	2210	-5	0.11	1.32±0.06
NGC 4278	55	7886	N4RW42	12:20:06.85	29:16:50.7	640	0.129	649	-5	0.07	...
NGC 4291	98	7886	N4RW69	12:20:17.80	75:22:14.3	640	0.160	1757	-5	0.17	...
NGC 4406	56	7453	N4HD03	12:26:11.75	12:56:47.7	384	0.128	-227	-5	0.35	1.61±0.16
NGC 4434	56	7453	N4HDA5	12:27:36.68	08:09:15.9	384	0.096	1071	-5	0.02	1.77±0.19
NGC 4458	56	7453	N4HDA3	12:28:57.59	13:14:31.3	384	0.103	671	-5	0.09	2.15±0.22
NGC 4472	56	7453	N4HD05	12:29:46.72	08:00:00.0	384	0.096	868	-5	0.19	1.52±0.14
NGC 4527	(56)	7331	N3ZD80	12:34:08.78	02:39:08.8	256	0.095	1734	+4	0.66	...
NGC 4536	(56)	7331	N3ZD0V	12:34:27.10	02:11:16.9	384	0.079	1804	+4	0.57	...
NGC 4565	235	7331	N3ZD0W	12:36:20.62	25:59:14.5	384	0.067	1227	+3	0.87	...
NGC 4589	98	7886	N4RW55	12:37:25.12	74:11:30.4	640	0.121	1980	-5	0.19	...
NGC 4594	...	7331	N3ZD86	12:39:59.40	-11:37:21.0	384	0.223	1091	+1	0.59	...
NGC 4636	152	7886	N4RW58	12:42:49.83	02:41:14.6	640	0.124	1095	-5	0.22	...
NGC 4709	59	7453	N4HD15	12:50:03.66	-41:22:56.8	1600	0.512	4624	-5	0.15	...
NGC 4725	(235)	7330	N3ZB98	12:50:26.79	25:30:05.4	640	0.051	1206	+2	0.29	...
NGC 5193	...	7453	N4HD11	13:31:53.26	-33:14:05.2	1920	0.242	3644	-5	0.07	...
IC 4296	225	7453	N4HD12	13:36:38.86	-33:57:55.9	1920	0.265	3871	-5	0.05	...
NGC 5273	...	7330	N3ZB16	13:42:08.53	35:39:13.9	640	0.044	1054	-2	0.09	...
NGC 5845	70	7886	N4RW67	15:06:00.78	01:38:00.6	640	0.233	1450	-5	0.35	...
NGC 7014	82	7453	N4HD13	21:07:52.04	-47:10:44.3	1600	0.142	4980	-4	0.17	...
NGC 7280	...	7331	N3ZD97	22:26:27.53	16:08:55.6	384	0.240	1844	-1	0.31	...
NGC 7331	...	7450	N41VB8	22:37:04.24	34:24:56.0	256	0.395	821	+3	0.65	...
NGC 7457	...	7450	N41VB9	23:00:59.91	30:08:41.3	256	0.229	824	-3	0.46	...
NGC 7743	...	7330	N3ZB49	23:44:21.68	09:56:03.6	640	0.296	1662	-1	0.15	...

^aGroups and clusters as defined by Faber et al. 1989 (Fornax=31, LeoI=57, Virgo=56); entries in parantheses are spirals not classified by Faber et al. but clearly belonging to a group or cluster.

^bB-band extinction from Schlegel et al. 1998

^cT-types and ellipticities from RC3; ellipticity $e = (1-b/a) = (1-10^{-\log R_{25}})$

^dKuntschner 2000, Kuntschner et al. 2000, and Trager et al. 2000

Table 2. Distances and F160W SBF Magnitudes

Galaxy	$(V-I)_0$ (mag)	$(m-M)$ (mag)	\overline{m}_{F160W} (mag)	\overline{M}_{F160W} (mag)	Dust	Ref ^a
NGC 7814	1.245±0.017	30.44±0.14	26.57±0.09	−3.87±0.17	D	<i>I</i> -SBF
NGC 221	1.133±0.007	24.39±0.08	19.11±0.05	−5.28±0.10	...	<i>I</i> -SBF
NGC 224	1.231±0.007	24.24±0.08	19.78±0.04	−4.46±0.09	...	<i>I</i> -SBF
		24.38±0.05	19.78±0.04	−4.60±0.06		new PL
		24.48±0.05	19.78±0.04	−4.70±0.06		new PL+Z
NGC 404	1.054±0.011	27.41±0.10	21.98±0.09	−5.43±0.13	...	<i>I</i> -SBF
NGC 524	1.221±0.010	31.74±0.20	27.19±0.20	−4.55±0.28	...	<i>I</i> -SBF
NGC 708	1.275±0.015	33.83±0.20	29.09±0.08	−4.74±0.22	D	HST <i>I</i> -SBF
NGC 821	1.196±0.022	31.75±0.17	27.03±0.09	−4.72±0.19	...	<i>I</i> -SBF
NGC 1052	1.213±0.010	31.28±0.27	26.51±0.07	−4.77±0.28	...	<i>I</i> -SBF
NGC 1172	1.112±0.032	31.50±0.20	26.57±0.09	−4.93±0.22	...	<i>I</i> -SBF
NGC 1316	1.132±0.016	31.50±0.17	26.11±0.09	−5.39±0.19	D	<i>I</i> -SBF
NGC 1351	1.148±0.016	31.45±0.16	26.68±0.05	−4.77±0.17	...	<i>I</i> -SBF
NGC 1339	1.134±0.012	31.45±0.35	26.43±0.07	−5.02±0.36	...	<i>I</i> -SBF
NGC 1344	1.135±0.011	31.32±0.30	26.26±0.07	−5.06±0.31	...	<i>I</i> -SBF
NGC 1365	1.153±0.028	31.18±0.10	25.64±0.09	−5.54±0.10	D	new PL
		31.27±0.05	25.64±0.09	−5.63±0.10		new PL+Z
NGC 1373	1.085±0.013	31.6 ±0.5	26.40±0.12	−5.2 ±0.5	...	<i>I</i> -SBF
NGC 1374	1.146±0.016	31.32±0.13	26.50±0.13	−4.82±0.18	...	<i>I</i> -SBF
NGC 1375	1.070±0.019	31.42±0.13	25.95±0.07	−5.47±0.15	...	<i>I</i> -SBF
NGC 1379	1.143±0.019	31.35±0.15	26.24±0.11	−5.11±0.19	...	<i>I</i> -SBF
NGC 1380	1.197±0.019	31.07±0.18	26.43±0.05	−4.64±0.19	D	<i>I</i> -SBF
NGC 1380A	1.138±0.018	30.84±0.29	26.16±0.16	−4.68±0.33	...	<i>I</i> -SBF
NGC 1381	1.189±0.018	31.12±0.21	26.55±0.10	−4.57±0.23	...	<i>I</i> -SBF
NGC 1386	1.101±0.018	30.93±0.25	25.81±0.06	−5.12±0.26	D	<i>I</i> -SBF
NGC 1387	1.208±0.047	31.38±0.26	26.0 ±0.8	−5.4 ±0.8	D	<i>I</i> -SBF
NGC 1389	1.145±0.019	31.52±0.18	26.36±0.08	−5.16±0.20	...	<i>I</i> -SBF
NGC 1399	1.227±0.016	31.34±0.16	26.79±0.04	−4.55±0.16	...	<i>I</i> -SBF
NGC 1400	1.170±0.009	31.95±0.33	27.17±0.08	−4.78±0.34	...	<i>I</i> -SBF
NGC 1404	1.224±0.016	31.45±0.19	26.69±0.08	−4.76±0.21	...	<i>I</i> -SBF

Table 2—Continued

Galaxy	$(V-I)_0$ (mag)	$(m-M)$ (mag)	\overline{m}_{F160W} (mag)	\overline{M}_{F160W} (mag)	Dust	Ref ^a
NGC 1426	1.161±0.009	31.75±0.18	26.88±0.06	−4.87±0.19	...	<i>I</i> -SBF
NGC 1427	1.152±0.018	31.70±0.24	26.42±0.05	−5.28±0.25	...	<i>I</i> -SBF
IC 2006	1.183±0.018	31.43±0.29	26.61±0.05	−4.82±0.29	...	<i>I</i> -SBF
NGC 1553	1.159±0.016	31.18±0.17	26.32±0.07	−4.86±0.18	...	<i>I</i> -SBF
NGC 3031	1.187±0.011	27.80±0.26	22.99±0.05	−4.81±0.26	...	<i>I</i> -SBF
		27.75±0.08	22.99±0.05	−4.76±0.09		new PL
		27.80±0.08	22.99±0.05	−4.81±0.09		new PL+Z
NGC 3032	1.073±0.019	31.55±0.28	26.05±0.10	−5.50±0.30	D	<i>I</i> -SBF
NGC 3056	1.073±0.023	30.27±0.25	25.48±0.07	−4.79±0.26	...	<i>I</i> -SBF
NGC 3351	1.225±0.014	29.85±0.09	25.19±0.07	−4.66±0.11	D	new PL
		30.00±0.09	25.19±0.07	−4.81±0.11		new PL+Z
NGC 3368	1.145±0.015	29.92±0.22	24.88±0.09	−5.04±0.24	D	<i>I</i> -SBF
		29.97±0.06	24.88±0.09	−5.09±0.11		new PL
		30.11±0.06	24.88±0.09	−5.23±0.11		new PL+Z
NGC 3379	1.193±0.015	29.96±0.11	25.26±0.08	−4.70±0.14	...	<i>I</i> -SBF
NGC 3384	1.151±0.018	30.16±0.14	25.34±0.17	−4.82±0.22	...	<i>I</i> -SBF
NGC 3928	1.096±0.015	31.0 ±0.6	25.60±0.09	−5.4 ±0.7	D	<i>I</i> -SBF
NGC 4143	1.181±0.015	30.85±0.19	26.68±0.06	−4.17±0.20	...	<i>I</i> -SBF
NGC 4150	1.071±0.017	30.53±0.24	25.60±0.13	−4.93±0.27	D	<i>I</i> -SBF
NGC 4261	1.258±0.014	32.34±0.19	28.04±0.11	−4.30±0.22	...	<i>I</i> -SBF
NGC 4291	1.175±0.017	31.93±0.32	27.66±0.08	−4.27±0.33	...	<i>I</i> -SBF
NGC 4278	1.161±0.012	30.87±0.20	26.38±0.09	−4.49±0.22	...	<i>I</i> -SBF
NGC 4406	1.167±0.008	31.01±0.14	26.26±0.06	−4.75±0.15	...	<i>I</i> -SBF
NGC 4434	1.125±0.015	31.98±0.17	26.78±0.12	−5.20±0.21	...	<i>I</i> -SBF
NGC 4458	1.140±0.011	31.02±0.12	26.03±0.05	−4.99±0.13	...	<i>I</i> -SBF
NGC 4472	1.218±0.011	30.90±0.10	26.26±0.04	−4.64±0.11	...	<i>I</i> -SBF
NGC 4527	1.23 ±0.03	30.53±0.09	25.43±0.07	−5.10±0.11	D	new PL/G&S ^b
		30.61±0.09	25.43±0.07	−5.13±0.11		new PL/G&S+Z
NGC 4536	1.20 ±0.07	30.80±0.04	25.46±0.12	−5.34±0.13	D	new PL
		30.87±0.04	25.46±0.12	−5.41±0.13		new PL+Z

Table 2—Continued

Galaxy	$(V-I)_0$ (mag)	$(m-M)$ (mag)	\overline{m}_{F160W} (mag)	\overline{M}_{F160W} (mag)	Dust	Ref ^a
NGC 4565	1.128±0.027	31.05±0.17	25.53±0.08	−5.52±0.19	D	<i>I</i> -SBF
NGC 4589	1.180±0.015	31.55±0.22	27.21±0.08	−4.34±0.23	...	<i>I</i> -SBF
NGC 4594	1.175±0.031	29.79±0.18	25.06±0.09	−4.73±0.20	...	<i>I</i> -SBF
NGC 4636	1.233±0.012	30.67±0.13	26.10±0.08	−4.57±0.15	...	<i>I</i> -SBF
NGC 4709	1.221±0.015	32.88±0.17	28.51±0.07	−4.37±0.18	...	HST <i>I</i> -SBF
NGC 4725	1.209±0.023	30.45±0.34	25.72±0.10	−4.73±0.35	...	<i>I</i> -SBF
		30.38±0.06	25.72±0.10	−4.66±0.12		new PL
		30.46±0.06	25.72±0.10	−4.74±0.12		new PL+Z
NGC 5193	1.208±0.015	33.35±0.15	28.52±0.06	−4.83±0.16	D	HST <i>I</i> -SBF
IC 4296	1.199±0.015	33.53±0.16	28.82±0.08	−4.71±0.18	D	HST <i>I</i> -SBF
NGC 5273	1.142±0.017	30.93±0.26	26.13±0.09	−4.80±0.28	...	<i>I</i> -SBF
NGC 5845	1.124±0.012	31.91±0.21	27.43±0.07	−4.48±0.22	...	<i>I</i> -SBF
NGC 7014	1.248±0.015	33.84±0.15	29.06±0.11	−4.78±0.19	...	HST <i>I</i> -SBF
NGC 7280	1.105±0.009	31.77±0.22	26.42±0.09	−5.35±0.24	...	<i>I</i> -SBF
NGC 7331	1.120±0.017	30.43±0.17	25.43±0.08	−5.00±0.19	D	<i>I</i> -SBF
		30.81±0.09	25.43±0.08	−5.38±0.12		new PL
		30.84±0.09	25.43±0.08	−5.41±0.12		new PL+Z
NGC 7457	1.104±0.009	30.45±0.21	25.57±0.09	−4.88±0.23	...	<i>I</i> -SBF
NGC 7743	1.080±0.009	31.42±0.17	25.99±0.06	−5.43±0.18	...	<i>I</i> -SBF

^a*I*-SBF=Tonry et al. 2001, shifted by −0.16 mag to the calibration derived using the Udalski et al. 1999 Cepheid period–luminosity relation; HST *I*-SBF=Jensen et al. 2001 and Lauer et al. 1998, also calibrated using the new period–luminosity relation; new PL=Freedman et al. 2001; new PL/G&S=Gibson & Stetson 2001; +Z indicates distances derived using a metallicity correction of −0.2 mag dex^{−1}.

^b The Cepheid period–luminosity relation and metallicity corrections used by Gibson & Stetson were the same as those used by Freedman et al. to determine the “new PL” and “new PL+Z” distances. The Gibson & Stetson distances assume a distance modulus for the LMC of 18.45 rather than the value of 18.50 adopted by Freedman et al. 2001. We have therefore added 0.05 mag to the Gibson & Stetson values.

REFERENCES

- Ajhar, E. A., Lauer, T. R., Tonry, J. L., Blakeslee, J. P., Dressler, A., Holtzman, J. A., & Postman, M. 1997, *AJ*, 114, 626
- Alonso, A., Arribas, S. & Martinez-Roger, C. 1996, *A&A*, 313, 873
- Alonso, A., Arribas, S. & Martinez-Roger, C. 1999, *A&AS*, 140, 261
- Bertelli, G., Bressan, A., Chiosi, C., Fagotto, F., & Nasi, E. 1994, *A&AS*, 106 275
- Bessell, M. S., Castelli, F., & Plez, B. 1998, *A&A*, 333, 231
- Blakeslee, J. P., Ajhar, E. A., & Tonry, J. L. 1999, in *Post-Hipparcos Cosmic Candles*, eds. A. Heck & F. Caputo (Boston: Kluwer Academic Publishers), 181
- Blakeslee, J. P., Vazdekis, A., & Ajhar, E. A. 2001, *MNRAS*, 320, 193
- Bruzual, G. & Charlot, S. 1993, *ApJ*, 405, 538
- Bruzual, G. & Charlot, S. 2002, in preparation
- de Vaucouleurs, G., de Vaucouleurs, A., Corwin, H. G., Buta, R. J., Paturel, G., & Fouque, P. 1991, *Third Reference Catalogue of Bright Galaxies* (New York: Springer-Verlag) (RC3)
- Caputo, F., Marconi, M., & Musella, I. 2002, *ApJ*, 566, 833
- Carretta, E., Gratton, R. G., Clementini, G., & Pecci, F. F. 2000, *ApJ*, 533, 215
- Faber, S. M., Wegner, G., Burstein, D., Davies, R. L., Dressler, A., Lynden-Bell, D., & Terlevich, R. J. 1989, *ApJ*, 69, 763
- Ferrarese, L. et al. 2000a, *ApJ*, 529, 745
- Ferrarese, L. et al. 2000b, *ApJS*, 128, 431
- Ferrarese, L., Silbermann, N. A., Mould, J. R., Stetson, P. B., Saha, A., Freedman, W. L., & Kennicutt, R. C., Jr. 2000c, *PASP*, 112, 117
- Freedman, W. & Madore, B. 1990, *ApJ*, 365, 186
- Freedman, W. et al. 1994, *ApJ*, 427, 628
- Freedman, W. et al. 2001, *ApJ*, 553, 47

- Girardi, L., Bressan, A., Bertelli, G., & Chiosi, C. 2000, *A&AS*, 141, 371
- Gibson, B. K. & Stetson, P. B. 2001, *ApJ*, 547, 103
- Gibson, B. K. et al. 1999, *ApJ*, 512, 48
- Gibson, B. K. et al. 2000, *ApJ*, 529, 723
- Graham, J. A. et al. 1997, *ApJ*, 477, 535
- Jensen, J. B., Luppino, G. A., & Tonry, J. L. 1996, *ApJ*, 468, 519
- Jensen, J. B., Tonry, J. L., & Luppino, G. A. 1998, *ApJ*, 505, 111
- Jensen, J. B., Tonry, J. L., & Luppino, G. A. 1999, *ApJ*, 510, 71
- Jensen, J. B., Tonry, J. L., Thompson, R. I., Ajhar, E. A., Lauer, T. R., Rieke, M. J., Postman, M., & Liu, M. C. 2001, *ApJ*, 550, 503 (J2001)
- Kennicutt, R. C., Jr. et al. 1998, *ApJ*, 498, 181
- Kuntschner, H. 2000, *MNRAS*, 315, 184
- Kuntschner, H., Lucey, J. R., Smith, R. J., Hudson, M. J., & Davies, R. L. 2000, *MNRAS*, 323, 615
- Lauer, T. R., Tonry, J. L., Postman, M., Ajhar, E. A., & Holtzman, J. A. 1998, *ApJ*, 499, 577
- Lejeune, T., Cuisinier, F., & Buser, R. 1997, *A&AS*, 125, 229
- Lejeune, T., Cuisinier, F., & Buser, R. 1998, *A&AS*, 130, 65
- Liu, M. C., Charlot, S., & Graham, J. R. 2000, *ApJ*, 543, 644
- Liu, M. C. & Graham, J. R. 2001, *ApJ*, 557, 31L
- Liu, M. C., Graham, J. R., & Charlot, S. 2002, *ApJ*, 564, 216
- Luppino, G. A. & Tonry, J. L. 1993, *ApJ*, 410, 81
- Mei, S., Kissler-Patig, M., Silva, D. R., & Quinn, P. J. 2001a, *A&A*, 376, 793
- Mei, S., Quinn, P. J., & Silva, D. R. 2001b, *A&A*, 371, 779
- Mei, S., Silva, D. R., & Quinn, P. J. 2001c, *A&A*, 366, 54

- Mochejska, B. J., Macri, L. M., Sasselov, D. D., & Stanek, K. Z. 2000, *AJ*, 120, 810
- Newman, J. A., Ferrarese, L., Stetson, P. B., Maoz, E., Zepf, S. E., Davis, M., Freedman, W. L., & Madore, B. F., 2001, *ApJ*, 553, 562
- Pahre, M. A. & Mould, J. R. 1994, *ApJ*, 433, 567
- Saha, A., Sandage, A., Labhardt, L., Tammann, G. A., Macchetto, F. D., & Panagia, N. 1996, *ApJ*, 466, 55
- Saha, A., Sandage, A., Thim, F., Labhardt, L., Tammann, G. A., Christensen, J., Panagia, N., & Macchetto, F. D., 2001, *ApJ*, 551, 973
- Schlegel D. J., Finkbeiner, D. P., & Davis, M. 1998, *ApJ*, 500, 525
- Stephens, A. W., Frogel, J. A., Ortolani, S., Davies, R., Jablonka, P., Renzini, A., & Rich, R. M. 2000, *AJ*, 119, 419
- Thompson, R. I., Storrie-Lombardi, L. J., Weymann, R. J., Rieke, M. J., Schneider, G., Stobie, E. & Lytle, D. 1999, *AJ*, 117, 17
- Tonry, J. L., Ajhar, E. A. & Luppino, G. A. 1990, *AJ*, 100, 1416
- Tonry, J. L., Blakeslee, J. P., Ajhar, E. A., & Dressler, A. 1997, *ApJ*, 475, 399
- Tonry, J. L., Blakeslee, J. P., Ajhar, E. A., & Dressler, A. 2000, *ApJ*, 530, 625
- Tonry, J. L., Dressler, A., Blakeslee, J. P., Ajhar, E. A., Fletcher, A. B., Luppino, G. A., Metzger, M. R., & Moore, C. B. 2001, *ApJ*, 546, 681
- Tonry, J. L. & Schneider 1988, *AJ*, 96, 807
- Trager, S. C., Faber, S. M., Worthey, G., & Jesus Gonzalez, J. 2000, *AJ*, 119, 1645
- Udalski, A., Soszynski, I., Szymanski, M., Kubiak, M., Pietrzynski, G., Wozniak, P., & Zebrun, K. 1999, *Acta Astron*, 49, 223
- Udalski, A., Wyrzykowski, L., Pietrzynski, G., Szewczyk, O., Szymanski, M., Kubiak, M., Soszynski, I., & Zebrun, K. 2001, *Acta Astron*, 51, 221
- Vazdekis, A. 1999, *ApJ*, 513, 224
- Vazdekis, A. 2001, *Ap&SS*, 276, 921
- Worthey, G. 1993, *ApJ*, 409, 530

Worthey, G. 1994, ApJS, 95, 107